AFRL-DE-
TR-2002-1050

Compact, High Power, Multi-Spectral Mid-Infrared Semiconductor Laser Package

Dr. Bujin Guo
Wen-Yen Hwang
Dr. Chih-Hsiang Lin

Applied Optoelectronics, Inc.
242 Kingfisher Dr
Sugar Land, TX 77478

October 2001

Final Report

AIR FORCE RESEARCH LABORATORY
Directed Energy Directorate
3550 Aberdeen Ave SE
AIR FORCE MATERIEL COMMAND
KIRTLAND AIR FORCE BASE, NM 87117-5776

REPORT DOCUMENTATION PAGE

Form Approved OMB No. 0704-0188

1. REPORT DATE (DD-MM-YYYY)	2. REPORT TYPE	3. DATES COVERED (FROM - TO)
01-10-2001		01-02-2001 to 31-07-2002

4. TITLE AND SUBTITLE
Compact, High Power, Multi-Spectral Mid-Infrared Semiconductor Laser Package
Unclassified

5a. CONTRACT NUMBER
5b. GRANT NUMBER
5c. PROGRAM ELEMENT NUMBER

6. AUTHOR(S)

5d. PROJECT NUMBER
5e. TASK NUMBER
5f. WORK UNIT NUMBER

7. PERFORMING ORGANIZATION NAME AND ADDRESS
Applied Optoelectronics, Inc.
242 Kingfisher Dr
Sugar Land, TX77478

8. PERFORMING ORGANIZATION REPORT NUMBER

9. SPONSORING/MONITORING AGENCY NAME AND ADDRESS
,

10. SPONSOR/MONITOR'S ACRONYM(S)
11. SPONSOR/MONITOR'S REPORT NUMBER(S)

12. DISTRIBUTION/AVAILABILITY STATEMENT
APUBLIC RELEASE
,

13. SUPPLEMENTARY NOTES

14. ABSTRACT
refer to atch

15. SUBJECT TERMS

16. SECURITY CLASSIFICATION OF:			17. LIMITATION OF ABSTRACT	18. NUMBER OF PAGES	19. NAME OF RESPONSIBLE PERSON
a. REPORT	b. ABSTRACT	c. THIS PAGE	Same as Report (SAR)	72	Mosher, Jan Janet.Mosher@kirtland.af.mil
Unclassified	Unclassified	Unclassified			19b. TELEPHONE NUMBER International Area Code Area Code Telephone Number DSN

REPORT DOCUMENTATION PAGE

Form Approved OMB No. 0704-0188

1. REPORT DATE (DD-MM-YYYY)	2. REPORT TYPE	3. DATES COVERED (FROM - TO)
01-10-2001		01-02-2001 to 31-07-2002

4. TITLE AND SUBTITLE
Compact, High Power, Multi-Spectral Mid-Infrared Semiconductor Laser Package
Unclassified

5a. CONTRACT NUMBER
5b. GRANT NUMBER
5c. PROGRAM ELEMENT NUMBER

6. AUTHOR(S)

5d. PROJECT NUMBER
5e. TASK NUMBER
5f. WORK UNIT NUMBER

7. PERFORMING ORGANIZATION NAME AND ADDRESS
Applied Optoelectronics, Inc.
242 Kingfisher Dr
Sugar Land, TX77478

8. PERFORMING ORGANIZATION REPORT NUMBER

9. SPONSORING/MONITORING AGENCY NAME AND ADDRESS
,

10. SPONSOR/MONITOR'S ACRONYM(S)
11. SPONSOR/MONITOR'S REPORT NUMBER(S)

12. DISTRIBUTION/AVAILABILITY STATEMENT
APUBLIC RELEASE
,

13. SUPPLEMENTARY NOTES

14. ABSTRACT
refer to atch

15. SUBJECT TERMS

16. SECURITY CLASSIFICATION OF:			17. LIMITATION OF ABSTRACT	18. NUMBER OF PAGES	19. NAME OF RESPONSIBLE PERSON
a. REPORT	b. ABSTRACT	c. THIS PAGE	Same as Report (SAR)	72	Mosher, Jan Janet.Mosher@kirtland.af.mil
Unclassified	Unclassified	Unclassified			19b. TELEPHONE NUMBER International Area Code Area Code Telephone Number DSN

Using Government drawings, specifications, or other data included in this document for any purpose other than Government procurement does not in any way obligate the U.S. Government. The fact that the Government formulated or supplied the drawings, specifications, or other data, does not license the holder or any other person or corporation; or convey any rights or permission to manufacture, use, or sell any patented invention that may relate to them.

This report has been reviewed by the Public Affairs Office and is releasable to the National Technical Information Service (NTIS). At NTIS, it will be available to the general public, including foreign nationals

If you change your address, wish to be removed from this mailing list, or your organization no longer employs the addressee, please notify AFRL/DELS, 3550 Aberdeen Ave SE, Kirtland AFB, NM 87117-5776.

Do not return copies of this report unless contractual obligations or notice on a specific document requires its return.

This report has been approved for publication.

ROB HILL, 2d LT
Project Manager

JEFFREY B. SALTER, CAPT.
Chief, Tactical Laser Branch

R. EARL GOOD, SES
Director, Directed Energy

REPORT DOCUMENTATION PAGE

Form Approved
OMB No. 0704-0188

1. REPORT DATE *(DD-MM-YYYY)*	**2. REPORT TYPE**	**3. DATES COVERED** *(From - To)*
October 2001	Final Report	1-Feb-01–31-Jul-02

4. TITLE AND SUBTITLE

Compact, High Power, Multi-Spectral Mid-Infrared Semiconductor Laser Package

5a. CONTRACT NUMBER
F29601-00-2-0058

5b. GRANT NUMBER

5c. PROGRAM ELEMENT NUMBER
63605F

6. AUTHOR(S)
Dr. Bujin Guo*
Wen-Yen Hwang
Dr. Chih-Hsiang Lin

5d. PROJECT NUMBER
3151

5e. TASK NUMBER
LP

5f. WORK UNIT NUMBER
AF

7. PERFORMING ORGANIZATION NAME(S) AND ADDRESS(ES)

Applied Optoelectronics, Inc.
242 Kingfisher Dr
Sugar Land, TX 77478

8. PERFORMING ORGANIZATION REPORT NUMBER

9. SPONSORING / MONITORING AGENCY NAME(S) AND ADDRESS(ES)

10. SPONSOR/MONITOR'S ACRONYM(S)

11. SPONSOR/MONITOR'S REPORT NUMBER(S)
AFRL-DE-TR-2002-1050

12. DISTRIBUTION / AVAILABILITY STATEMENT

Approved for public release; distribution is unlimited

13. SUPPLEMENTARY NOTES

*University of Houston
4800 Calhoun Rd
Houston, TX 77204

14. ABSTRACT

Through a vertically integrated effort involving atomic level material engineering, advanced device processing development, state-of-the-art optomechanical packaging, and thermal management, Applied Optoelectronics, Inc. (AOI), University of Houston (UH), and Physical Science, Inc. (PSI) have made progress in both Sb-based type-II semiconductor material and inP-based type-I laser device development. We have achieved record performance on InP based quantum cascade continuous wave (CW) laser (with more than 5 mW CW power at 210 K). Grating-coupled external-cavity quantum cascade lasers were studied for temperatures from 20 to 230 K. A tuning range of 88 nm has been obtained at 80 K. The technology can be made commercially available and represents a significant milestone with regard to the Dual Use Science and Technology (DUST) intention of fostering dual use commercial technology for defense need. AOI is the first commercial company to ship products of this licensed technology.

15. SUBJECT TERMS

Type I Quantum Cascade Laser 5.2 μm, Sb-based Type II Quantum Cascade Laser

16. SECURITY CLASSIFICATION OF:			**17. LIMITATION OF ABSTRACT**	**18. NUMBER OF PAGES**	**19a. NAME OF RESPONSIBLE PERSON**
a. REPORT	**b. ABSTRACT**	**c. THIS PAGE**			2d Lt Robert Hill
Unclassified	Unclassified	Unclassified	Unlimited	72	**19b. TELEPHONE NUMBER** *(include area code)* (505) 846-5094

TABLE OF CONTENTS

FIGURES

TABLES

1.0 Summary

The objective of this project is to develop a technology for compact, portable, thermoelectrically (TE) cooled mid-infrared semiconductor laser sub-systems to provide a platform for applications that require power, brightness, multi-spectral capability, and modulation flexibility. The project was organized into a vertically integrated effort involving laser material development, advanced device configuration, state-of-the-art optomechanical packaging, and thermal management. Applied Optoelectronics, Inc. (AOI) has been the prime contractor and leader of the team. Within the past 18 month, we have made many progress in both Sb-based type-II semiconductor material and InP-based type-I laser devices, especially the record performance on InP based quantum cascade CW laser. The technology can be made commercially available and represents a significant milestone with regard to the Dual Use Science and Technology (DUST) intention of fostering dual use commercial technology for defense need. AOI is the first commercial company to ship products of this licensed technology.

The first two quarters had been focused on the material development and design improvements. Despite several encounters of MBE machine problems, we have grown more than 50 laser wafers. We have made great effort to develop the best laser device processing technology and implemented many quality control procedures during wafer processing and device development. The wet chemical etching of the Sb-based materials have been refined to be both inexpensive and production-compatible. The AR/HR coating procedure has been developed in house. New facilities have been added to produce the good quality of laser die and sub-mount. The prototype TE-cooled package housing has been made and the TE-cool systems are evaluated. The thermal modeling work has been carried out both in-house and with the collaboration with an external source. At the same time, laser characterizing test laboratory has been optimized with the new testing equipments. An LABVIEW based data collection and analysis software systems have been developed. In parallel, system development from other programs, including mid-IR code-division multiplexing lidar, and tunable external cavity laser were available as a platform to provide support and guidance for this component development effort.

Beginning in the third quarter, we have explored the possibility of developing this technology with both Sb-based Type II Quantum Cascade(QC) laser and the Type I QC laser in 5.2 μm laser structures. The material development of type I QC laser provide us with better performance at 5.2 μm wavelength region. The better laser performance was achieved through improved material quality and careful thermal engineering of the laser structure to reduce the temperature rise of the laser's active region during cw operation. We have made some progress in other areas such as laser material improvement, advanced device processing, as well as the laser device characterization.

In the fourth to sixth quarters, we have achieved some great results with our type-I quantum cascade laser technology. Continuous-wave (cw) operation up to 210 K (-63 ºC), approximately 35 degrees higher than the best previously published results, reported by Lucent Technologies in 1999. This is the highest cw operating temperature for semiconductor lasers above 3 μm. This milestone was achieved through improved material quality and careful thermal engineering of the laser structure to reduce the temperature rise of the laser's active region during cw operation. In addition, a differential absorption lidar system has actually been demonstrated at a lower laser power level and shorter range in another synergistic program, and helps establish this program concept feasibility ahead of schedule. More important is a novel system design recently developed that allows more advanced and higher functionality than that in the original proposal. This system architecture is based on code-division multiplexing (CDM), and requires every channel be programmable for an adaptive intelligence at the sensor level. At large distance with weak signal intensity, all channel signals can be operated with the same code for optimum signal-to-noise ratio. At closer range, the channels can be split into different bands for target spectral recognition. The process can be iterative, splitting into finer spectral granularity until a target positive identification is achieved. Such an adaptive intelligence is similar to the biological eye/optical nervous system that optimizes intensity and color signals for target recognition.

AOI perceives that its mission of a commercialized technology of mid-IR lasers is within reach, and the realization of the market is a long-term process depending on new technical and business development. The current business environment of a highly competitive photonics sector also demands AOI to respond to the market pressure with a focused strategy on resources, products, and technology. Consequently, while University of Houston is still pursuing their own technical tasks, AOI will shift its resources to other projects, and will gradually reduce its own assigned tasks within this program. AOI has produced or is currently producing a quantity of materials and devices that will be sufficient for the revised program objectives and assigned tasks for the program partners, which have a programmed time lag relative to AOI's tasks. AOI will thus finish its technical involvement of the program on August 31 2001.

The key results and major progress we have achieved in this time period based on the main task areas of the program are summarized in Table I.

Table I. Summary of the progress

Material development Objective: To produce high quality laser wafer	The material growth development include several focus: Type-II material growth of OP and EP wafers Type-I μm quantum cascade laser structures growth
Device development Objective: To optimize laser devices.	Our effort of device development has focused on the following areas: Device simulation and modeling. Processing optimization including etching processing, facet coating, dielectric and metal film deposition. DFB grating fabrication with both e-beam lithography and in-house holographic lithographic facility. Building of new facilities including processing clean rooms and new equipments
Packaging & integration Objective: To produce a turn-key package for potential application	The packaging and integration development are focused on: Compact, TE-cooled packaging design. Thermal modeling of the device with epi-down mounting that provide a better thermal management give us a record high temperature cw mode performance. The new laser device has demonstrated more than 8 milliwatts of cw power at a temperature of -63 ºC (-81 F).
System evaluation Objective: To evaluate the package for system application	Laser characterizing of the mounted device has been tested with different temperatures and currents. The optimized epi-down device mounting has set a record of highest CW operating temperature. Applications of integrating the laser device into a DIAL system has been evaluated and some excellent results has been demonstrated.

2.0 Program Status

Due to the reasons as stated earlier, an early mid-term project design review (PDR) was scheduled and some modification to the technical approaches and efforts are being made. The PDR involved an assessment and re-examination of the technical and business opportunities that were not anticipated at the beginning of the program and appeared during the program. The outcome of the work suggests that a modified technical approach can be pursued to achieve not only the same original objectives, which is a technology for compact mid-infrared (3-5 μm) semiconductor laser technology with scalability in power, brightness, multi-spectral capability, and modulation flexibility, but also an enabling technology for more advanced and novel system applications which is the ultimate spirit of the program. The PDR result suggests a revision that includes the evaluation and adaptation of many aspects of the telecom technology to exploit the technical advances as well as the economy of scales of this industry.

3.0 Material and technical development

The goal of this project is to develop a mid-IR semiconductor laser technology for applications that require power, brightness, wavelength diversity, and modulation flexibility. Examples of these applications include IR countermeasures, spectroscopic sensing, and covert surveillance. Spectroscopic sensing has potential applications in both defense and commercial market. These applications have been demonstrated for many years with a variety of experimental mid-IR laser sources such as gas lasers (CO, CO_2, DF, HF, …), solid state OPO, semiconductor lasers, and free-electron lasers. But a challenge is to realize a laser subsystem that can meet realistic system requirements, which consist not only of technical specifications such as power, brightness, wavelength, and modulation, but also practical aspects such as size, weight, power consumption, reliability, robustness, and even cost and manufacturability.

Mid-IR semiconductor lasers are attractive thanks to the practical advantages that have been proven for the related near-IR semiconductor lasers. Though not as mature, mid-IR semiconductor lasers have shown promising progress in recent years. Semiconductor materials based on III-V elements can now be used to generate long-wavelength, mid-IR light. The Sb-based interband laser has shown the best results in the 2-4.5 μm range [1-24], and the intraband quantum cascade approach has been best demonstrated from 3-10 μm. The InP-based quantum cascade (QC) lasers invented in 1994 have been making progress in the wavelength range of ~4-17 μm [25-30]. High-power Sb-laser prototypes have actually been developed for infrared countermeasure demonstration, but requiring mechanical coolers with substantial size and weight [4,6]. Work remains to be done to achieve high power and efficiency at a sufficiently high temperature that can use cost-effective, practical cooling technology such as thermoelectric.

3.1. Material development

Wafer Growth

The strategy of this project in regard to material development is not to engage in material research but only in material development. As the goal of the project is to achieve a product, proven material approaches will serve as the starting baseline. The project will not pursue high-risk approaches that are to be explored by a concurrent material research program, but it will exploit the best and latest know-how from the program. This is possible since the same group of personnel will be involved in both programs. The material development resource will be spent on obtaining high quality wafers by refining and optimizing the growth of proven recipes. As break-through and new understanding are conceivably achieved during the course of the project, the effort will adopt the best option.

Extensive technical development on type-I quantum cascade and on type-II Sb mid-IR semiconductor lasers has been published. For type-II materials, the challenge is to reduce the internal loss due to carrier absorption, and to increase the internal emission efficiency by suppressing the leakage current. The performance of the earlier type-II device is more than an order-of-magnitude lower than the fundamental limit, and calculation indicates that >5-times improvement is feasible. For this project, only 2~3 times improvement is necessary to achieve the goal of 0.1-W average power. The program effort includes intensive growth, extensive test and diagnostic measurement, and theoretical modeling of the laser physics. An advanced concept is to utilize tensile strain to shift the light hole band above the heavy hole band, resulting in transverse magnetic (TM) laser output. The internal loss can be very low for high power efficiency. However, the growth of this type of material is very high risk. More generally, the compatibility between the design and growth is always a major concern.

Lastly, the material thermal property is also critical. Thin cladding incurs high modal loss, but some cladding structure such as superlattice has low thermal conductivity and is not optimal for thermal management. Material design is thus linked to the packaging, and optimum design requires accurate determination of various trade-off.

The material development is also focused on refinement of the InP-based type-I QC laser structure we have been growing. The active region of the 5.2 μm InGaAs/InAlAs quantum cascade laser structure was grown lattice-matched on 2-inch epi-ready n+ InP substrates by molecular beam epitaxy. Arsenic and phosphorus valved cracker sources were used to provide the group V fluxes. The core of the structure consisted of 25 stages. Each stage comprised a three-quantum-well active region and a superlattice injection/relaxation region. Because of the phosphorus cracker, we were able to use InP as top cladding to take advantage of its higher thermal conductivity than the traditional InAlAs

We have grown both superlattice (SL) laser structure of 3.3 μm wavelength and the type-II quantum cascade (QC) laser structure of 4 μm. In addition, we also optimized the material growth of type-I InP based semiconductor laser structure. The growth also been listed in Appendix A.

Material characterization

As mentioned before, we have used X-ray, high magnification microscope, SEM, and AFM to check the wafer quality.

High resolution X-ray diffraction has been proved to be a powerful tool for the non-destructive ex-situ investigation of epitaxial layers. The composition and uniformity of the epitaxial layers, their thickness, the build-in strain and strain relaxation, and the crystalline perfection related to their dislocation density information can be obtained from the diffraction patterns. We use the X-ray to study the material composition,

thickness as well as the strain information. The cross wafer growth uniformity has also been studied. Figure 1a is a typical x-ray data for a good grown superlattice wafer. The cladding InAs/AlSb superlattice layer are clearly shown with its periodicity. Figure 1b shows a type-I QC laser wafer.

Optical microscopy is one of the most versatile and useful instruments in semiconductor characterization. We use an Olympus Normaski optical microscope for wafer surface morphology and defect evaluation. Figure 2 is a typical surface photograph of a grown wafer.

Ellipsometry measures the change in polarization state of light reflected from the surface of a sample. The measured values are expressed as *psi* and *delta.* These values are related to the ratio of Fresnel reflection coefficients, R_p and R_s for *p*- and *s*-polarized light, respectively. Because ellipsometry measures the ratio of two values, it can be highly accurate and very reproducible. Single layer InGaAs or InAlAs epi-grown on InP substrate was measured with a J. A. Woollam Co. variable angle spectroscopic ellipsometer (VASE®). All data were acquired and analyzed using WVASE32 software. Figure 3 is the fitting results of the Psi Component of the spectroscopic ellipsometry measurement of the InGaAs epi-layer. We can see that the experimental results fitted very well with the modeling.

AFM pictures are used to understanding the wafer surface morphology, Figure 4 is an example of the AFM image of a InAs/InGaSb SL surface. Using the high- resolution images obtained from AFM, we can easily identify the defects and any impurity particles and provide the necessary information for material improvement.

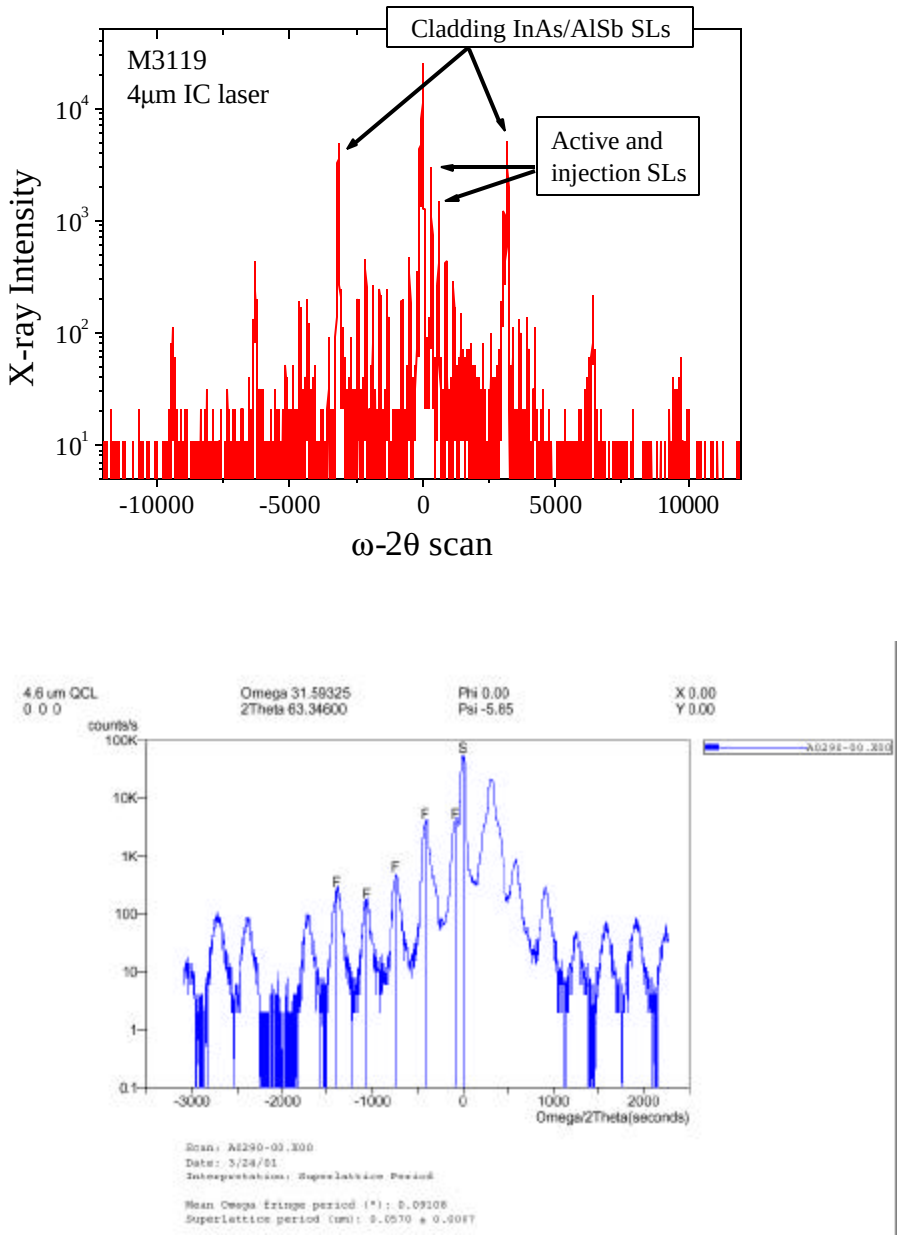

Figure 1. (a). X-ray data of a type-II cascade laser, (b). x-ray data of a type-I QC laser.

Figure 2. Nomarski photograph of a portion of the wafer shows the wafer surface morphology. The image was taken at 200X magnification.

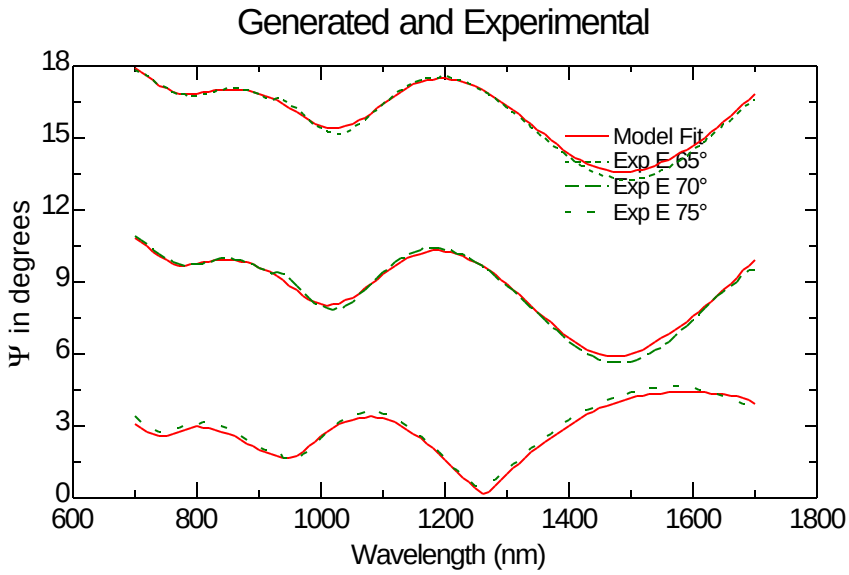

Figure 3. The modeling of the spectroscopic ellipsometry measurement of the InGaAs sample grown by MBE

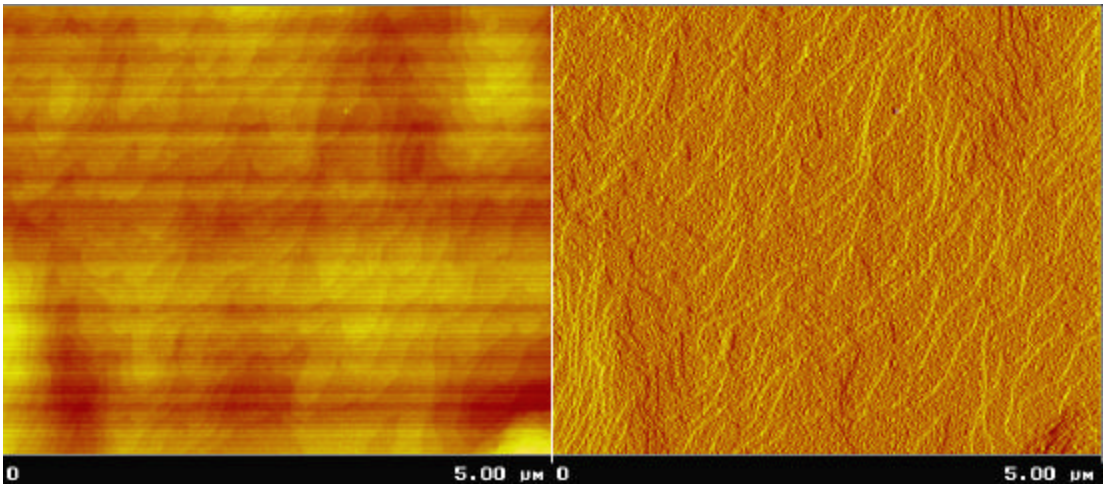

Photoluminescence data provide the valuable information about OP laser wafers. We can use the PL measurement to check out the laser wavelength and wafer uniformity even before processing. Figure 5 demonstrates a typical PL measurement.

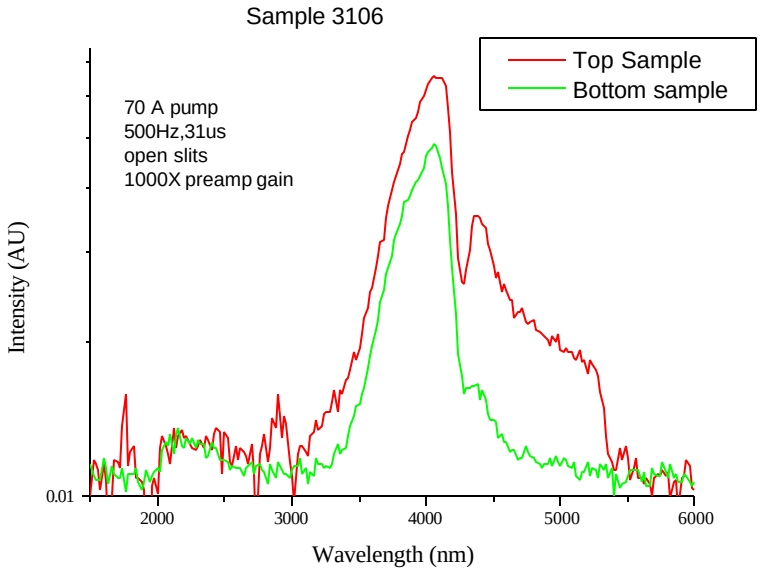

Wafer mapping

Among the analytical methods especially suitable for thin films, x-ray diffraction (XRD) plays an important role since it is nondestructive, no contact and highly quantitative. We use Phillip's X'Pert analytical x-ray system with the X'Pert Data Collector and X'Pert Epitaxy data analysis software. In the high-resolution mode, this system has a 12 arc-sec angular divergence of the primary beam can be achieved by using a four-crystal Ge monochromator, allowing for the investigation of thin films and multilayered systems with high crystalline quality.

Since the wafer was rotated during MBE growth, we can assume that the wafer characteristics would maintain a radial symmetry. Therefore, we only made the mapping along one direction – the radial. The mapping was performed in every 4 mm along the radius direction for five points. Figure 6 is a typical ω-2θ rocking curve mapping of a 2-inch wafer.

From the x-ray mapping, we can measure the grown laser structure superlattice thickness at every point. Since we have repeated laser structures in the design, it can be treated as supperlattice in the Phillip X'Pert to obtain the thickness for each repeated period. The result of a typical wafer measurement is demonstrated in Figure 7 where we can see that thickness of the laser structure is decreasing from center to edge. The actual thickness for one period is changed from 579 A at the center to 550 A at 16 mm from center.

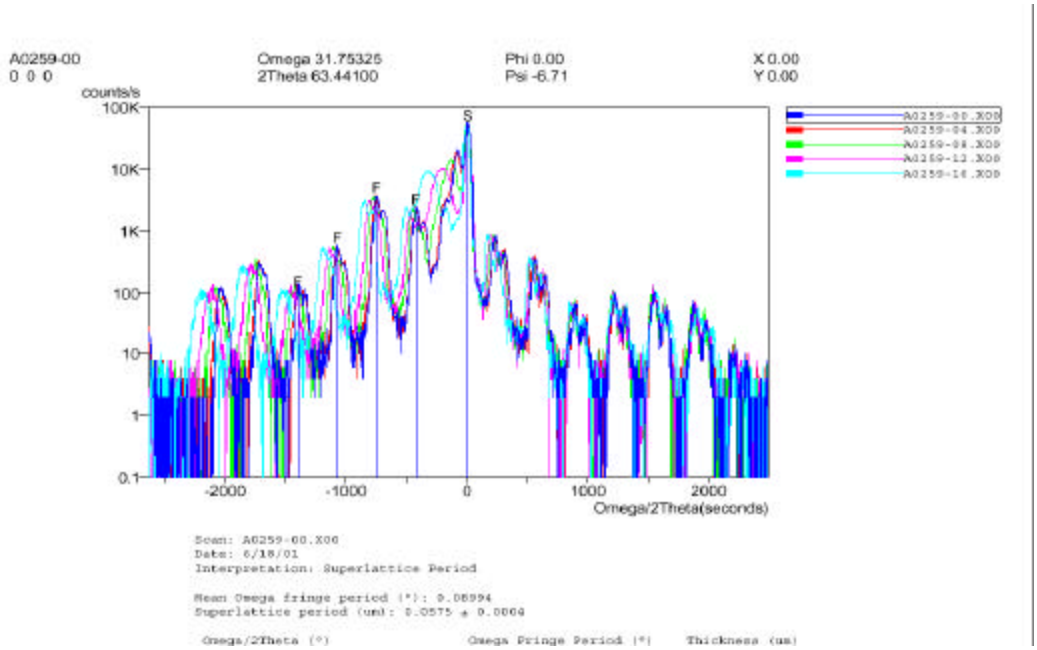

Figure 6. A typical ω-2θ rocking curve mapping of a 2-inch wafer.

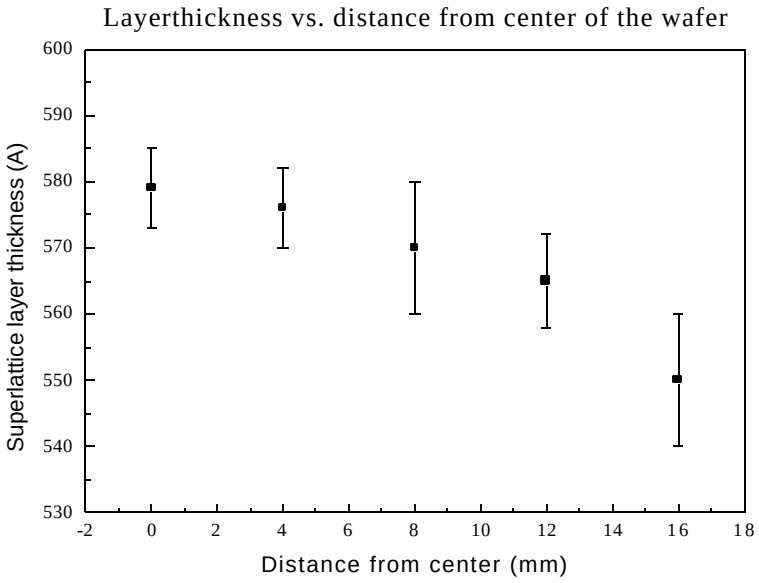

Figure 7. Layer thickness measured from the x-ray data plotted against the distance from the center of the wafer.

3.2. Simulation and modeling

Simulation

The theoretical calculations have been carried out with the simulation of the Superlattice (SL) active region. Figure 8 demonstrates the band diagram with the number of the periods of the active region substantially reduced for the sake of clarity. The designed structure was grown by MBE and the devices were tested.

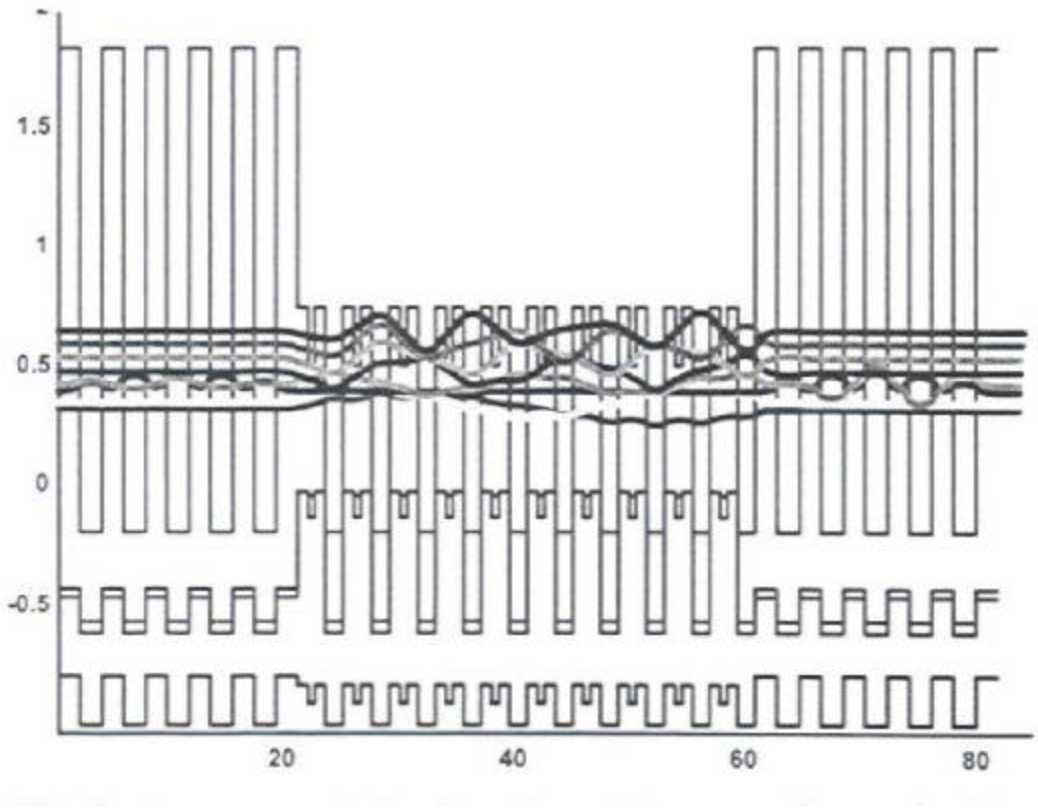

Figure 8. A representative bandgap diagram of a superlattice (SL) laser. Both the active and cladding regions are composed of SL.

In order to obtain the type-I multi-color quantum cascade laser transitions in the mid-IR region, we first try to simulate the laser transition using the 4.6 μm structure. Using a Matlab simulation program, we can calculate the energy levels and the wavefunctions. Figure 9 is a portion of the schematic energy diagram of the conduction band of the 5.2 μm type-I QC laser structure with the calculated wavefunctions.

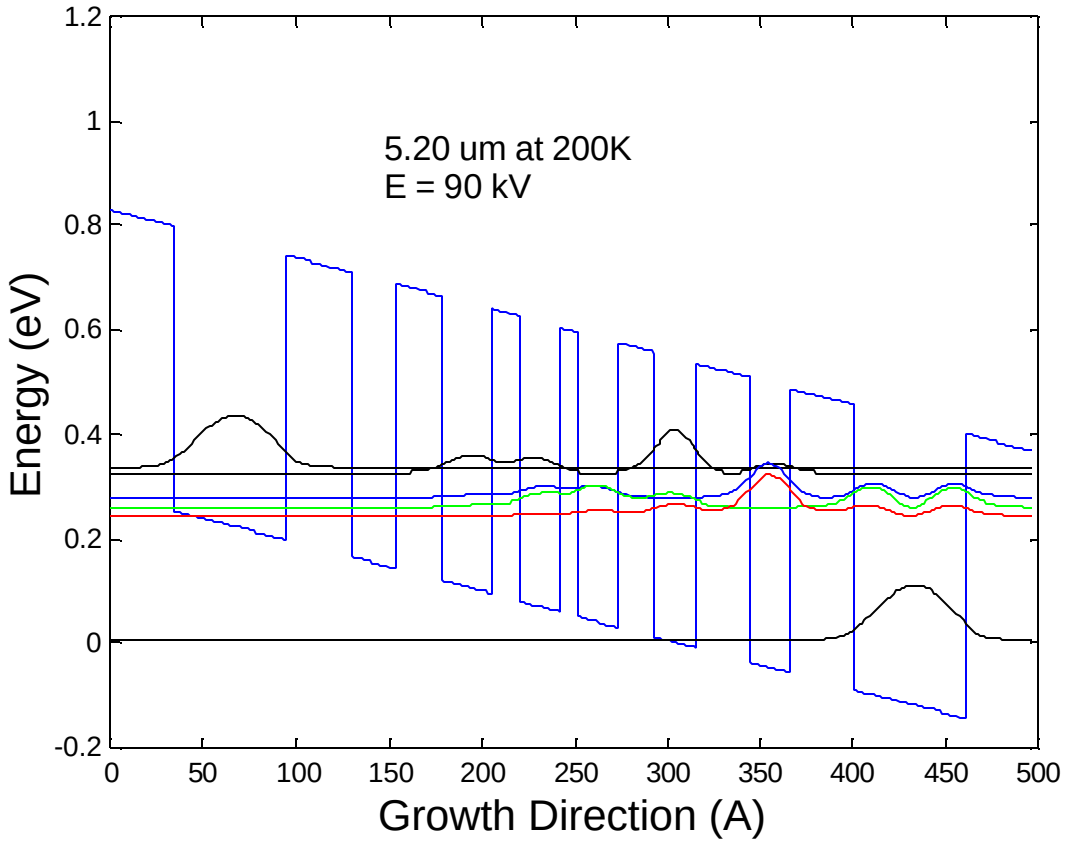

Figure 9. Simulated results of a symmetric quantum well structure at two opposite electrical fields.

Thermal modeling

The two dimensional thermal properties of the quantum cascade laser device have been simulated by a software package developed using MATLAB program environment. A finite element algorithm is used to solve the second order differential equation.

Figure 10a is the plot of thermal contour plot in steady state of a 10μm wide x 5.5μm device, deep etched type-I QC lasers mounted epi-up with 20 kW/cm^2 power density. Figure 10b shows the grid used to calculate the 2D temperature profile.

The die, mostly InP, is green, the copper sub-mount is red and a thin 2μm thick Indium layer is yellow. For the simulation, the bottom of the copper sub-mount is held at a constant temperature of 120 K. Note that the copper sub-mount is only ~5mm x 5mm. It was found that there is very little difference in the temperature profile in the die if a larger copper sub-mount is used. So, to speed up the calculations, the copper sub-mount was only made of the size shown above.

The simulations of a 10um wide device were performed with the laser mounted epi-up and epi-down, 40 kW/cm^2 of power applied, steady state, 120K heat sink temperature. Epi-down mounting lowers peak active region temperature by as much as 55 K. Figure 11 shows the temperature versus depth taken in the center of the 10μm wide stripe

We also simulated devices having a stripe of 6, 8 and 10μm wide epi-up mounting. The peak active region temperature is decreased by ~25 K for the 6μm device compared to the 10μm device. Figure 12 demonstrates the temperature profile along the center of the stripe.

a) b)

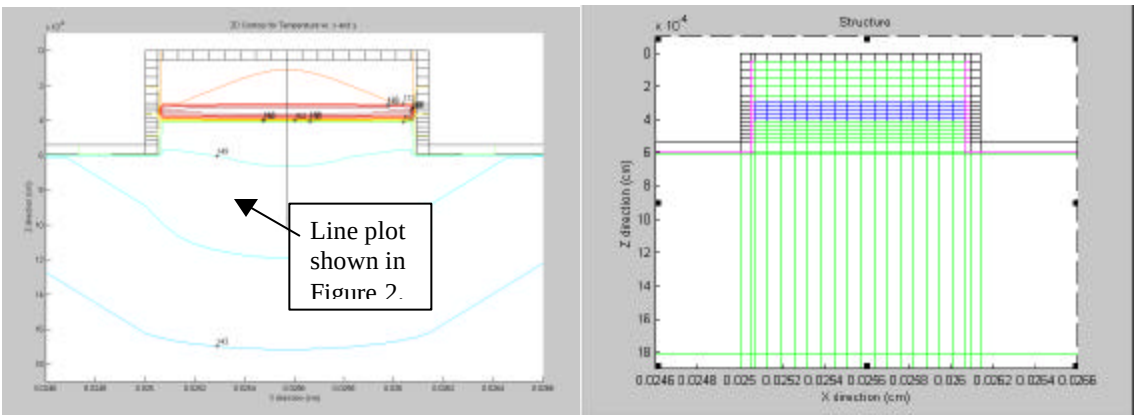

Figure 10. (a) Thermal contour plot in steady state. (b) the grid used to calculate the 2D temperature profile in a. Colors designate material: Black – Au, Magenta – SiO_2, Green – InP, Blue – active region.

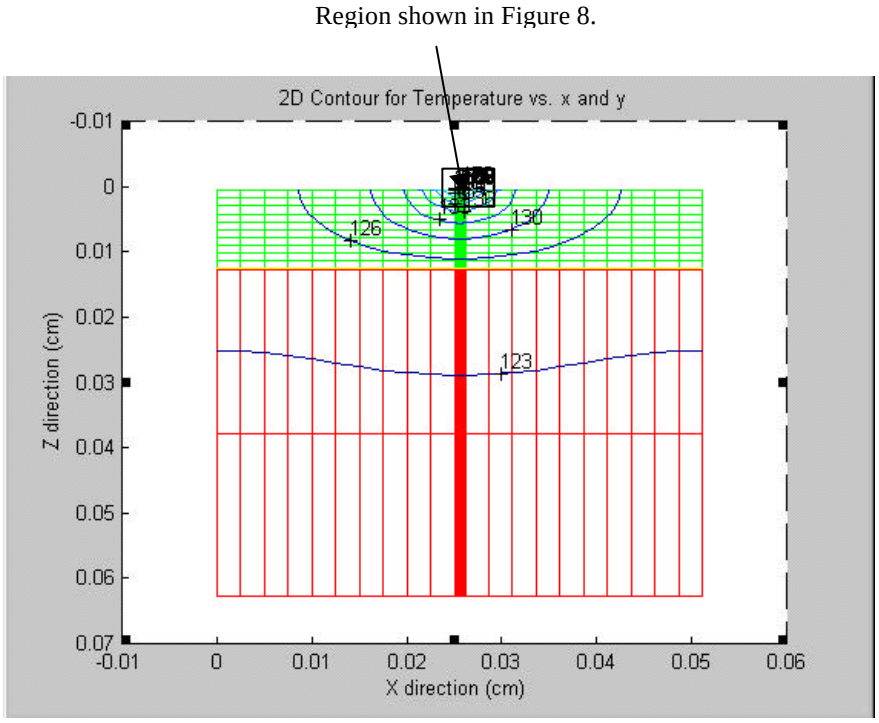

Figure 11. The entire grid used to calculate the thermal contour plot.

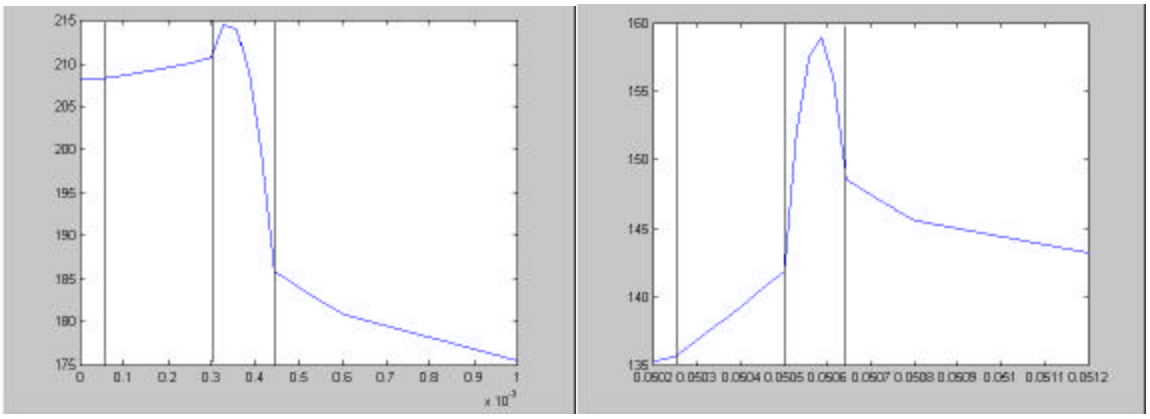

Epi – up Epi - down

Figure 12. Simulation results of the epi-up (left) and epi-down (right) mounting shows the center of the 10µm wide stripe. Structure: From left to right Au, Clad, Active, Clad/Substrate

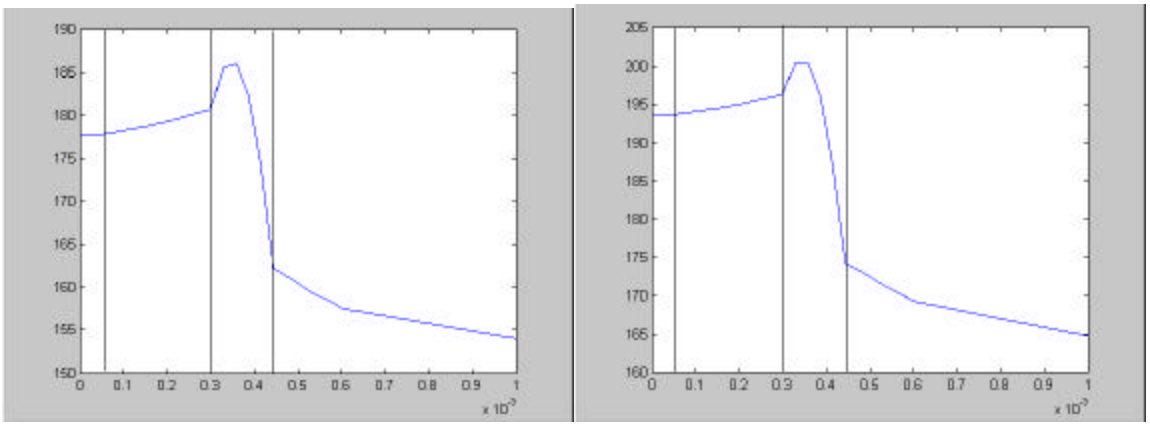

Epi-up, 6µm wide Epi-down, 8µm wide

Figure 13. Simulation results of the epi-up mounting of the different stripe width. Left: 6 µm; right: 10 µm. Structure: From left to right Au, Clad, Active, Clad/Substrate

It can be seen in Figure 13 that the temperature in the active region reaches almost 190 K with 20 kW/cm^2 CW power applied. This is a fairly low power and corresponds to a current density of only 2.5 kA/cm^2 (if we assume a working voltage of 8V).

3.3. Device development

The device development strategy is to adopt approaches with minimal manufacturing complexity but sufficient to meet the goal. Extensive device concepts have been developed for the near-IR diode laser. But the internal loss and efficiency problems for the Sb laser are also radically different from that of the near-IR. Judiciousness is essential in evaluating the existing near-IR laser paradigm. As discussed above, it is desirable to set a goal in material development to reduce the problem to a level comparable to that of the near-IR. But the problem is rooted in a fundamental physical process (intervalence band absorption) which is not easily solvable. It is unrealistic to set the achievement of such a goal as a precondition for the success of this project. The device development strategy must then be based on realistic internal loss and efficiency problems.

Two basic device geometry, edge-emitter and grating-coupled surface-emitter are evaluated, each with unique merits. The edge-emitter geometry is well proven, and the majority of commercial near-IR diode lasers employ ridge-waveguide or broad-area geometry. A reason for their success is the progress in packaging and facet treatment technology that improve their power and brightness. These simple lasers steadily encroach onto the records of more complicated but also more costly device structures, which loose the cost-benefit competitiveness. But for the Sb, the edge-emitter is not without limitation. As shown in the development of high-power Sb-based prototype [4,22], thermal-loading consideration necessitates large devices. As an edge-emitter output efficiency is scaled as $(1/L)\ \mathrm{Log}(1/R)$ with R being the facet reflectivity, it decreases rapidly vs. device length L. Because of the large output divergence and the high film thickness required for coating in this wavelength range, anti-reflection coating is not trivial for the edge-emitting lasers. Among the best value for a 2-layer AR facet coating of 4-um semiconductor lasers is ~ 3 – 4% [10,22]. These limitations result in an upper limit and trade-off for the net power efficiency, output, and scaling option. As shown in the reference, a long device (3-mm) has a higher maximum power output than that of a 2-mm device because of less thermal

loading, but has a poorer power efficiency than that of the short device. An option for improvement is to design a large optical cavity to reduce the output divergence for a more effective antireflection coating. However, this also entails significant risk in the material growth.

Etching optimization

Etching process is the first crucial step to make the laser mesa structure for edge emitting lasers. Currently, we are using wet chemical etching process. We have tested many different etching recipes for Sb-based laser materials. Finally, we are able to produce the high quality mesa etching as shown in Figure 14.

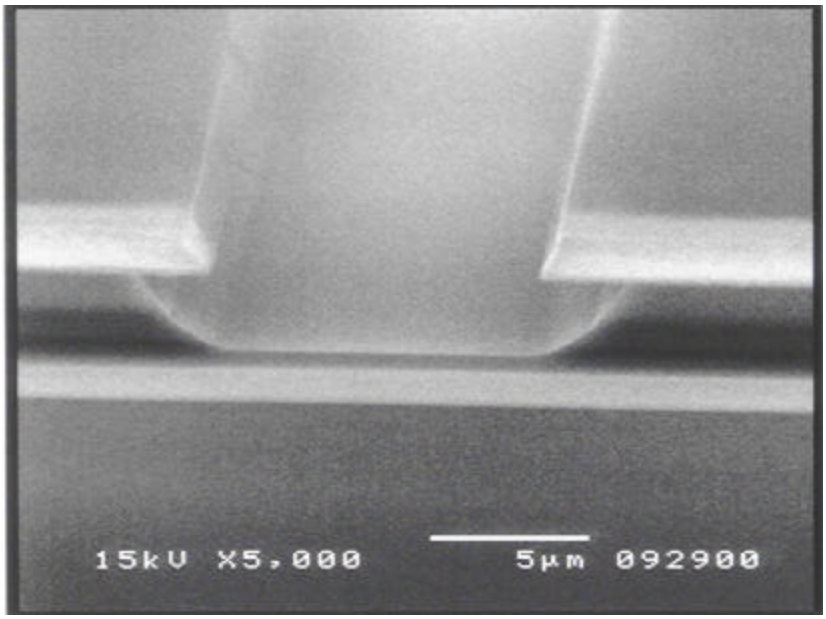

SiO_2 and Metal contact deposition.

The SEM images of the cleaved samples also demonstrated very good SiO_2 deposition (as shown in Figure 15).

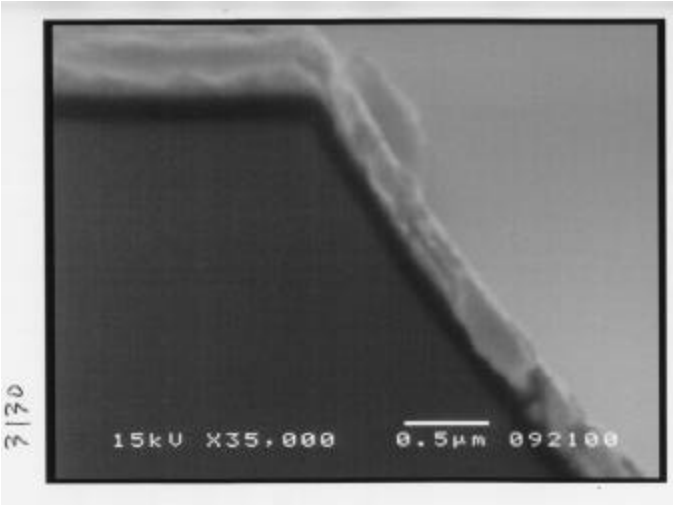

Figure 15. SEM image of the cleaved mesa edge demonstrates the SiO_2 deposition (Darker layer) between semiconductor and metal.

During the device processing, we have the problems of metal adhesion between GaSb and metal contact layer from time to time. Therefore, experiments have been designed and carried on to solve this problem. First of all, we try to eliminate the possibility of solvent contamination by using fresh solvent for every processing. Secondly, we have tested Ammonium sulfide treatment, which seems helped the metal adhesion to some extent. We also have tested annealing under different conditions (temperature and duration). The metal contact is able to survive the wire bonding process. The ohmic contact study is also under investigation. There is a very good Ohmic contact study done by a German group using Ti/Pd/Pt/Au which shows better result than that of Ti/Pt/Au for p-type GaSb. We will perform this study with several different metal/alloy combination soon.

Dielectric coating development

To test our coating system, Si films were deposited to determine the optical properties of the films. We deposited the silicon films at 15Å/s, 25 Å/s and 50 Å/s on double side polished GaAs. FTIR transmission spectra were taken over a range of 2µm to 15µm. A commercial optical thin film software was used to fit the optical constants (n, k) of the Si films in the wavelength range of 2 to 10 microns. Unfortunately the software proved to be unable to fit the FTIR transmission spectra for the optical constants.

The fits would not converge and give realistic optical constants. Various filters were applied to smooth the data and reduced data sets (reduced wavelength ranges) were tried but the fits would not converge to realistic values. The optical constants obtained in the fits did not reproduce the data. In addition, the software had problems fitting simulated data generated from itself. Therefore we stopped this approach to fit this data and we have characterized the optical films with ellipsometry and reflectance measurements. Also in the month of August, we have deposited 1 HR (2 layer) film for test purposes and coated 4 different samples with AR films. The AR films consisted of a single layer of Al_2O_3 of 1968 Å thickness. These AR films produced a minimum reflectivity of a few percent at the lasing wavelength and a low reflectivity (<20%) for the pump beam.

We deposited 3 test AR films and 7 laser coatings (4 AR and 3 HR films were deposited on different laser structures). The reflectance measurements of the AR and HR coated samples were compared to simulations calculated from the optical constants used in the ellipsometry program. The reflectance data agrees relatively closely with the simulations indicating that the optical constants used were close to the optical constants of the deposited materials. Figure 16 is a representative reflectance spectrum of a witness sample with the simulation for comparison. The AR coating is a single layer of Al_2O_3 at 1968 Å thickness.

The HR film was a 2 layer Si/ Al_2O_3 structure designed to be highly reflecting in the mid IR. The reflectance maximum is about 80%. The HR films are designed to cover a range of mid IR wavelengths. Figure 17 is a reflectance spectrum for a witness sample. The reflectance measurement was taken with an FTIR at 45º incidence. For reference, the simulation has been plotted showing the reflectance of the s and p polarizations.

The HR maximum occurs as a broad peak around 4.6 μ demonstrating how this design can cover a range of wavelengths as shown in Figure 19.

A 6444 Å Al_2O_3 film and a 6860 Å Si film were deposited at Applied Optoelectronics and were characterized with an IR-VASE® ellipsometer at the J A Wollam Company.

The data were fit for the optical constants n and k. Figure 18 are the plots of the optical constants from 2 to 30 μm.

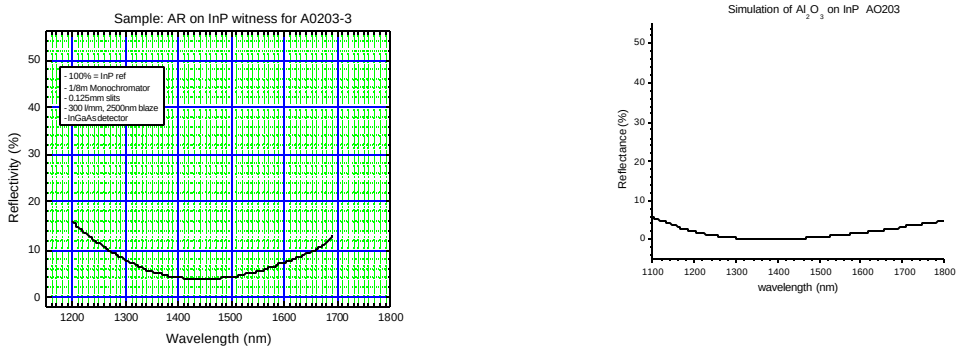

Figure 16. Reflectance spectra of the witness samples of AR coating.

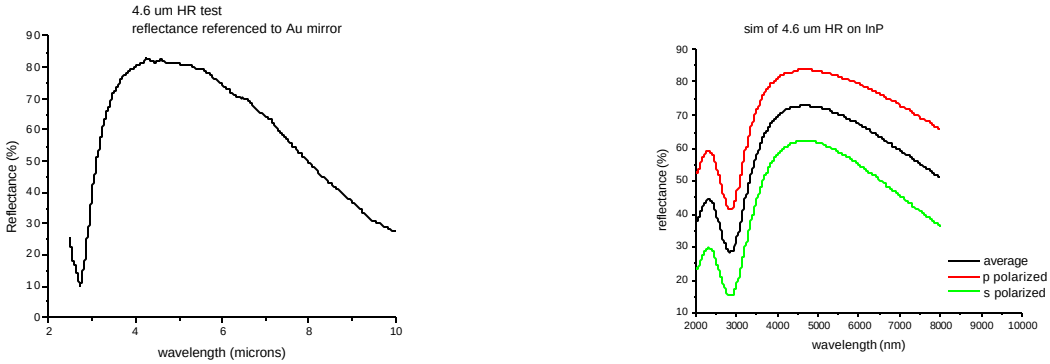

Figure 17. Reflectance spectra of the witness samples of HR coating.

In addition to the optical film depositions, the optical coating system also had maintenance to fix electronic power supply and vacuum problems (replaced cryo pump). The Si crucible was changed back to graphite. The Si would completely wet the Mo crucible, lifting the crucible up and resulting in a variable thermal contact. The variable thermal contact resulted in an unstable Si deposition rate. The graphite crucible gives a more uniform rate. The cracking of the crucible was solved by reducing the sweep of the electron beam to a small area inside the crucible.

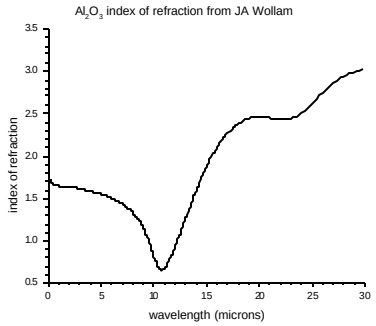

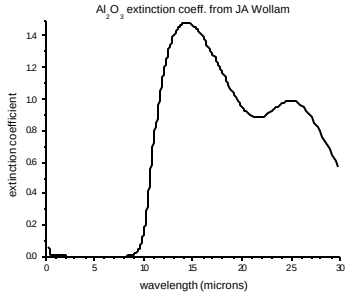

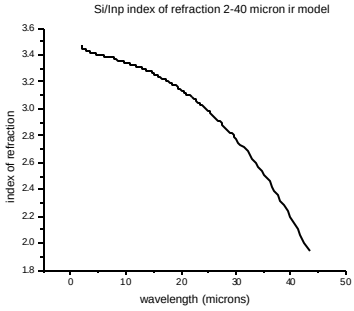

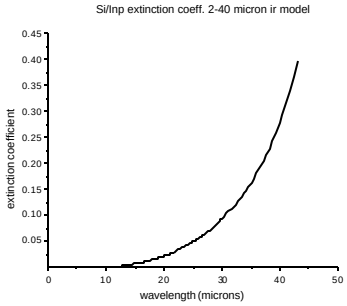

After the initial test, we deposited 9 test films and 1 AR and 2 HR films on laser structures. The AR coating is a single layer Al_2O_3 of 1968 Å thickness. The 2 HR coatings are a 3 layer Si/ Al_2O_3/Si structure. The Si layer next to the laser facet is thin and provides protection from oxidation of the facet during deposition. Test films of Si and Al_2O_3 were deposited to map out the deposition parameter envelope. The films were deposited at 5, 10 and 15 Å/s and about 4000 Å thick. The substrate temperature varied between 50ºC and 210ºC for the Al_2O_3 films and 40ºC and 110ºC for the Si films. Ellipsometry spectra were taken using a visible light ellipsometer. The data for the Al_2O_3 films were fit for thickness and optical constants using a Cauchy formula ($A + B/\lambda^2 + c/\lambda^4$). Using the fitted parameters, the optical constants for the Al_2O_3 films were extrapolated out to 2 microns and agree with the IR data. The Si ellipsometer data are still being fit. The optical constant data will be used in calculating the thickness of the layers in the AR and HR coatings.

X-ray diffraction mapping was done on the test depositions to map out effects due to stress in the films. Stress in the film will result in the substrate curvature. This curvature results in the diffraction peak occurring at a different angle. The data has been plotted out and are being analyzed. One test deposition of Al_2O_3 of 1955Å thickness was made. The reflectivity of the film was measured to be ~1% at the minimum.

In addition to the optical film depositions, a RGA was added to the system to monitor the gases during deposition. The main residual gas species is water and is typical of systems that are not extensively baked. The system is only given mild bakes to protect the laser samples from overheating. The current source-sample configuration of the system also results in significant heating of the sample from the source material. The temperature can rise as high as 160°C depending on the layer being deposited. The problem is a result of a source to sample distance that is too close. We are looking at installing a cooler that will

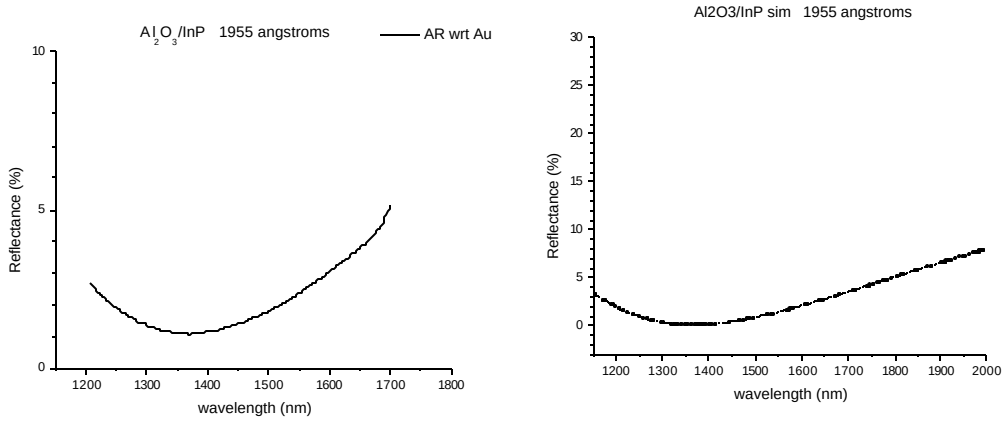

Figure 19. Reflectance spectra of the witness samples of HR coating.

increase the source to sample distance by 8 inches. We should gain an additional 2 inches with modifications to the sample holder. This should reduce the heating effect to below 70°C. The laser bar holder has been designed to mount different sizes of laser bars (cavity length and bar length). This design holds the laser bar between a block and a spring-loaded plate. This allows the laser bar cavity length and laser bar length to vary. Also, the design has been refined to reduce the amount of handling of the laser bars during mounting. Laser bar holders are being designed that will handle standard size laser bars with minimal handling, particulate generation and damage to the facet.

DFB grating development

Grating pattern written with e-beam lithography form Cornell nano-fabrication facility has been tested on wafer 3013. The result indicated that while etching on a test wafer could have decent quality, the etching on an actual wafer could be worse as shown in the

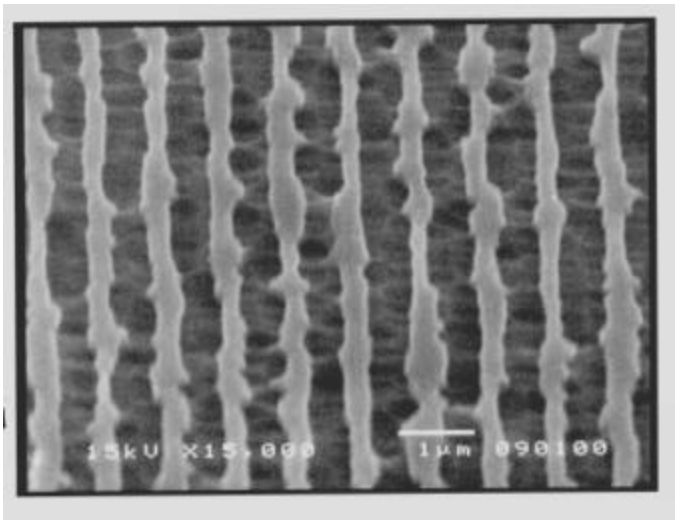

Figure 20. Etched grating pattern.

side Fig. 20. The problem was believed to be caused by the specific quality of the top cladding layer of sample #3013, which had occurred during the growth. Therefore, the effort to develop grating is postponed until the material growth issue is resolved. Nevertheless, the work indicated that e-beam lithography could be useful in the short term for development and testing. In the longer term, holographic grating will be more cost-effective.

The DFB grating has been fabricated on the device by contact mask method in the effort produce single mode lasers. Figure 21 is a SEM photograph of the grating on the surface. Since the contact mask technology can only produce the grating for a single structure design and the lead time and cost are not favorable for manufacturing setup, we are currently exploring the holographic lithographic technology for DFB grating development.

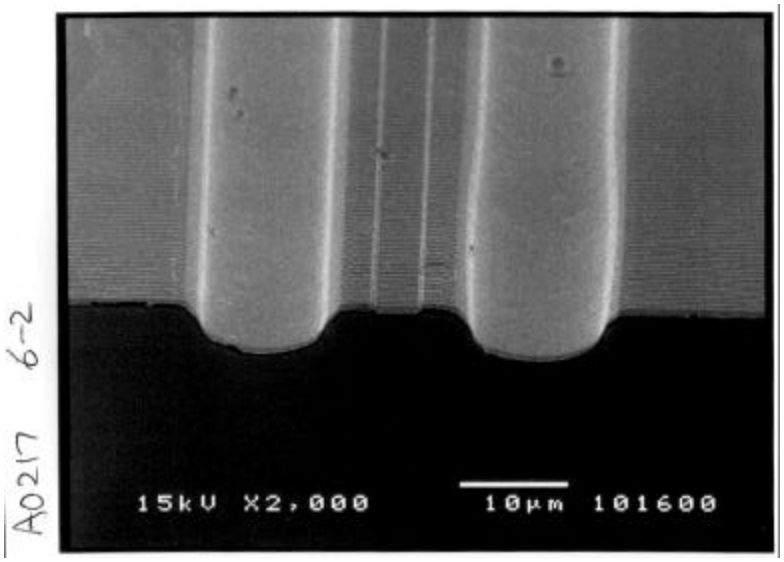

Figure 21. SEM photograph of the surface of the DFB laser .

Holographic lithography development

In our holographic exposure design, the wafer to be processed is coated with photo-resist and exposed to two incident plane waves as illustrated in Figure 22. An argon laser with an intra-cavity etalon for long coherence length is operated on either the 488.0 nm or 457.9 nm lines. The 457.9 nm wavelength is preferred since it gives the photoresist much greater sensitivity and shorter exposure time despite the lower power.

The actual setup schematic is demonstrated in Figure 23. The argon laser operating at 457.9 nm with a long coherent length is directed through a remotely controlled beam shutter and reflected by a high reflector to the spatial filter. After pass through the spatial filter, the expanded laser beam is being redirected by another high reflector to the 1.5 m focal length, 6" diameter high reflector mirror to form the highly collimated coherent beam. Half of the collimated beam are reflected by the 6"X3" mirror to overlap with another half beam to for the interference pattern on the wafer.

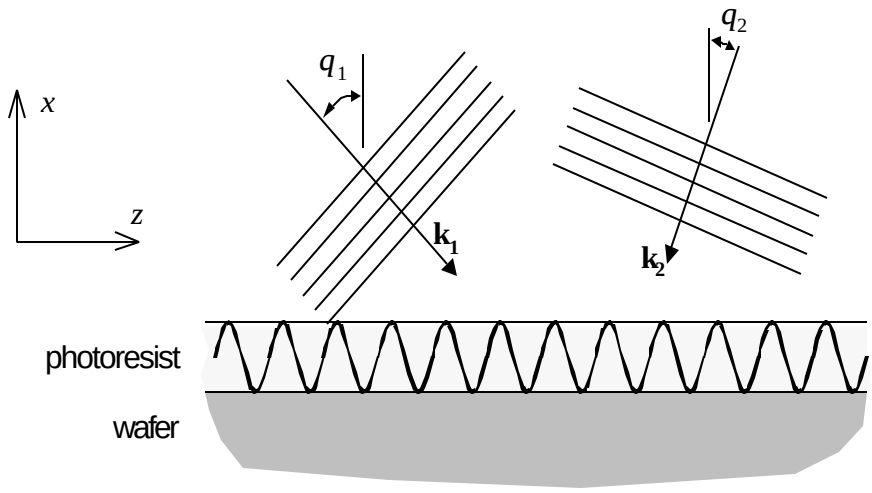

Figure 22. Holographic grating exposure technique. Two incident wavefronts interfere to create a standing wave in a layer of photoresist

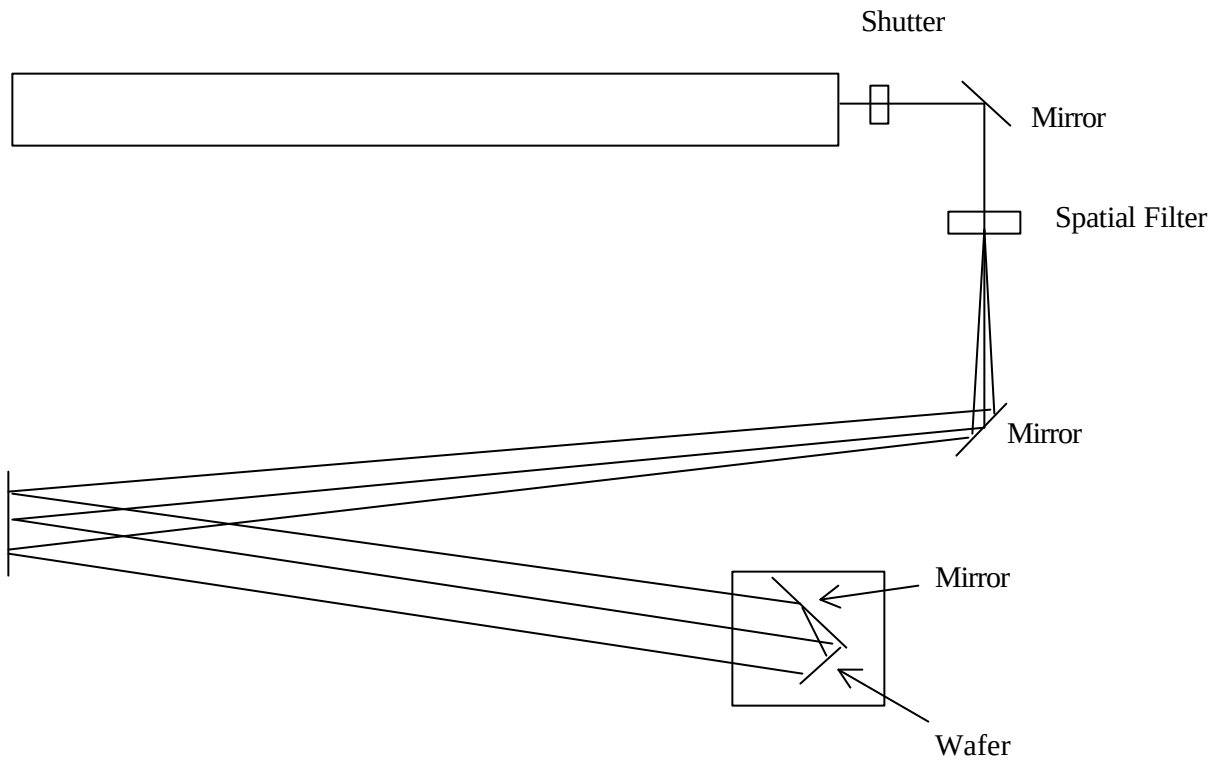

Figure 23. Holographic grating lithographic exposure setup schematic diagram.

Processing facility development

In November, 2000, AOI has completed the first phase of its move into the company's new manufacturing facility located in Sugar Land, Texas. AOI's new 24,000 sq. ft. manufacturing facility will consolidate the fast-growing company's administrative offices, laboratories and three production lines in one headquarters. The new facility was specially designed for the company and includes 10,000 sq. ft. of class 1,000 and 10,000 clean room space to house the company's array of advanced semiconductor crystal growth and processing equipment. Laboratories, additional production equipment, and office space for more than 100 employees occupy the remaining space.

All of our equipment have been moved to a new facility. The four photographs following demonstrate the processing equipment and the clean room facility at AOI.


S-3000N

3.4. Packaging and Integration

Packaging Facility

Like the processing facility, we have also installed several major packaging equipments and new facility for packaging. The photograph of a dicing machine is demonstrated here.

Prescreening of the diced device

In order to improve the yield of the processing and packaging, we have designed and assembled a simple test platform which allows quick and easy laser die testing at room temperature before mounting the die to a sub-mount. We have found that one can reliably pick up a die from a waffle pack, place it on a test stand then place a probe on the die without damaging the die. The device can be electrically pumped while monitoring for emission using a LN2 cooled InSb detector. Initial problems with the probe contact have been solved and the test jig appears to work well. The threshold current can be quickly determined, typically in less than 2 minutes per device and with some additional work it may also be possible to determine the slope/differential efficiency and IV curve as well.

Prototype package submount and housing

A design of new submount, which allows high frequency modulation and convenient operation with TE cooler, is shown in Figure 24a. It also allows high heat load. Figure 24b demonstrates the prototype TE-cooled package housing.

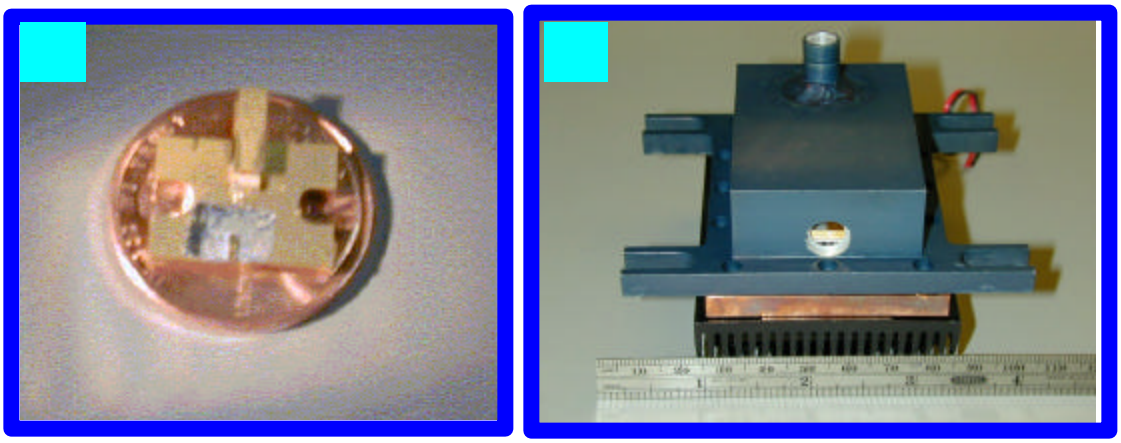

Epi-down packaging

Following cleaving and dicing, the device was mounted epi-side down on a copper submount. Therefore, several wafers that were processed with deep trench 8, 10, 12 and 16µm wide fabry-perot cavities have been diced and prescreened using the previously mentioned technique. We have mounted the samples epi-down and wire bond directly to the substrate. The samples mounted onto H-mounts with 2µm of Indium (did not use flux). The samples appeared to be bonded well and the front facet of those samples are un-scratched by the epi-down mounting.

4.0 Achievements on device technology

4.1. CW operation at 210K

The newest generation quantum cascade laser developed by AOI has demonstrated continuous-wave (cw) operation to a temperature of 210 K (-63 C) [31], approximately 35 degrees Celsius higher than the previous record, held by Lucent Technologies. Engineers achieved this milestone through improved material quality and careful thermal engineering of the laser structure to reduce the temperature rise of the laser's active region during cw operation. This accomplishment makes the quantum cascade laser a preferred technology for sensitive, spectroscopic chemical detection. Applications that require accurate analysis of trace gases, such as non-invasive medical diagnostics, industrial process control and environmental monitoring, stand to benefit from this technology.

The epi-down mounted 5.2μm type I QCL device was tested with the same setup as reported before. Briefly, A CRYOMECH cryostat with a home designed cold-finger which can mount 6 sub-mounted laser devices is employed. Temperatures are measured with two Si-sensors on cold-finger and a good thermal contact was assured every time when the sub-mounts are attached to the cold-finger. We use an Agilent 6644A system power supply running at constant current (CC) mode to provide the continuous DC current to the laser device. A software based on LABVIEW has been developed for experiment control and data acquisition. L-I curves shown in Figure 25 demonstrated that the laser device has excellence performance in CW mode. A record high temperature CW mode operation has been created with this device. We obtain ~8 mW of output power at 210 K! Although some rather peculiar characteristics in the L-I curve still need to be understood. We think that it might be mode hopping. More investigation is under way for better understanding and improving.

The threshold current density has been plotted at different temperatures in Figure 26. Assuming that the actual active region is 12 μm wide, we found that the characteristic temperature of T_0 is between 40 K and 325 K.

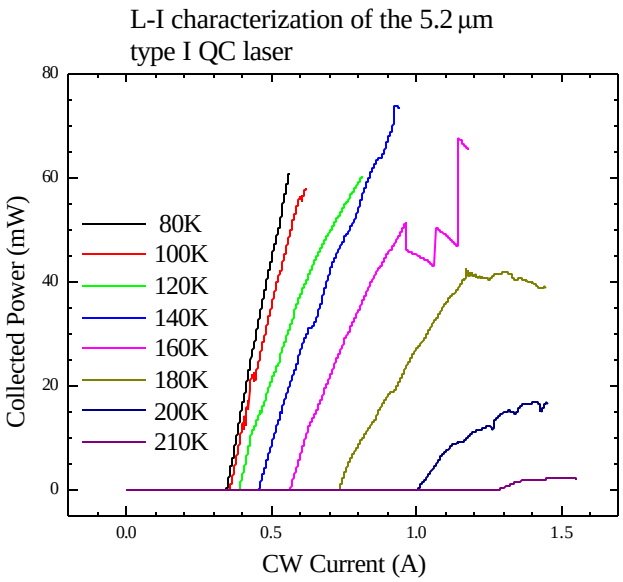

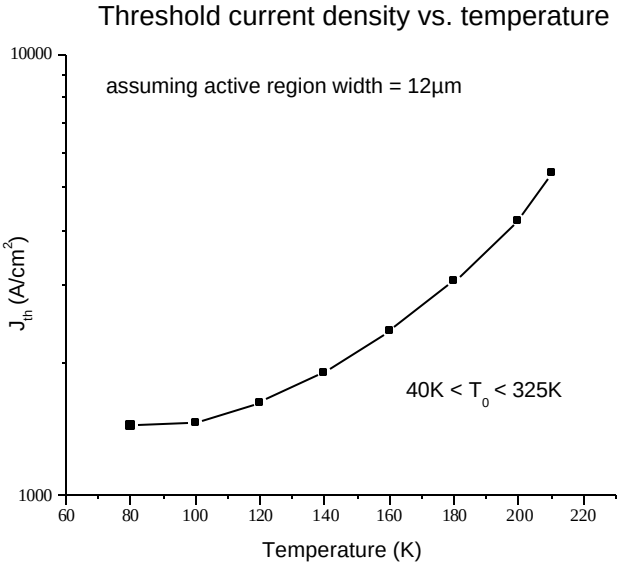

Using the assumption that the laser core temperature under pulsed operation is the same as the heat sink temperature and that the threshold current density depends only upon core temperature, the CW core temperature, T_{core}, can be determined by finding the pulsed mode heat sink temperature that gives the same threshold current density as in CW mode. The thermal resistance, R_{th}, between the core and the heat sink can then be calculated using

$$R_{th} = \frac{(T_{core} - T_{\sin k})}{V_{op} J_{th} A}$$

where T_{sink} is the CW heat sink temperature, V_{op} is the CW operating voltage at threshold, J_{th} is the CW threshold current density and A is the device area. Using this, the thermal resistance of our device was calculated to be 10.1 ± 0.1 K/W between 180K and 210K.

The lasing spectra of the laser device at various temperatures have been measured with a half-meter monochromator coupled with an liquid nitrogen cooled InSb photodiode detector. The spectra of different submount temperatures of the measured device are shown in Figure 27. The spectral wavelengths at different temperatures are shown in Figure 28.

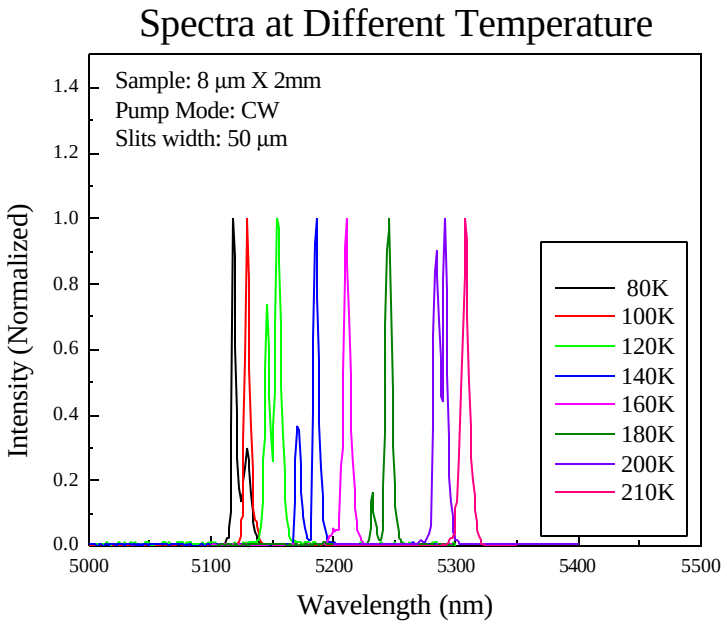

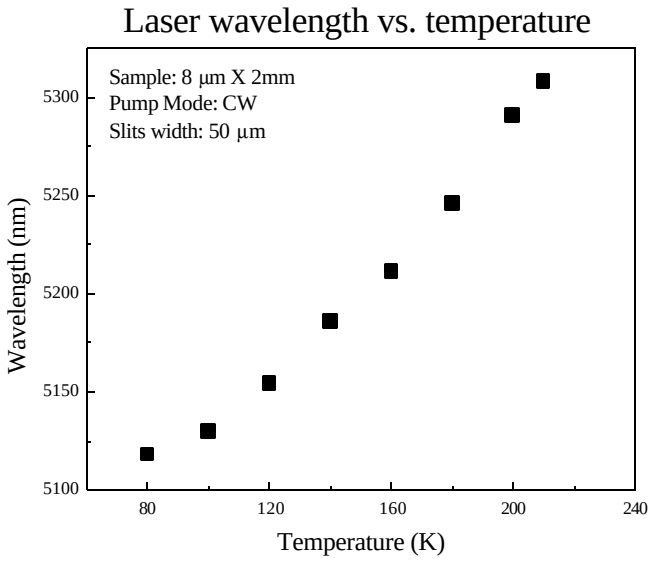

Figure 28. lasing wavelength vs. cryostat temperature at CW mode pumping

4.2. QC laser characterization

L-I characterization

L-I characterization of the Optically Pumped (OP) type-II lasers

The optically pumped laser devices were tested by pumping with 980 nm diode laser. Figure 29 shows the typical efficiency vs. temperature behavior from 80 K to 220 K. the results show that the laser wavelength is consistent with the laser design. However, the internal loss is quite high even at low temperature suggests that the material quality still needs to be improved.

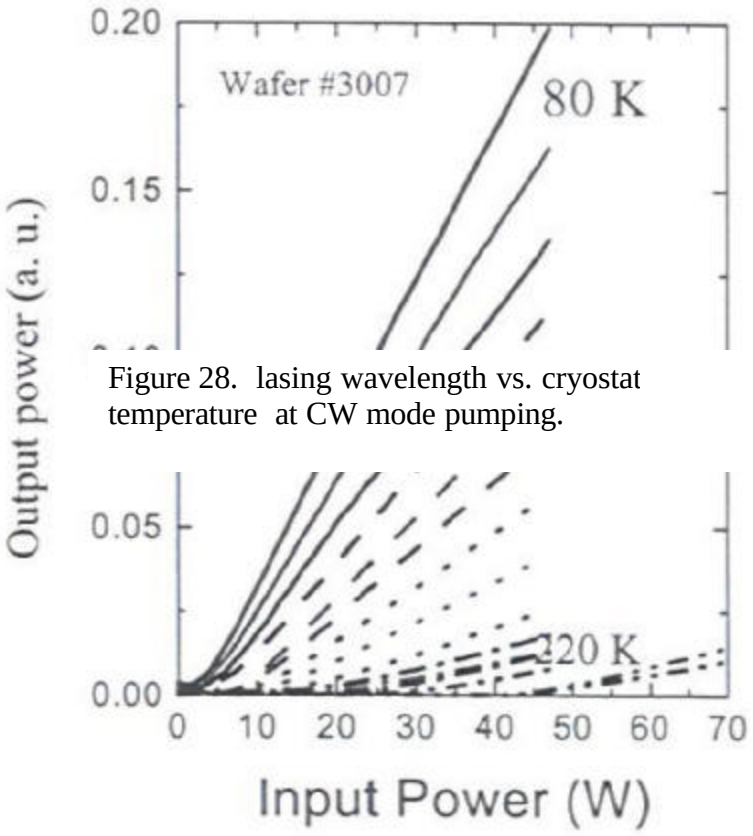

Figure 28. lasing wavelength vs. cryostat temperature at CW mode pumping.

Figure 29. Output power of OP lasers from Wafer 3007 for temperatures from 80 K to 220 K.

L-I characterization of the Electrically Pumped (EP) type-II lasers

The EP type-II laser structures have been grown and passed our qualification testing (X-ray, SEM, AFM etc.). Several of them have been processed to Fabry-Perot type edge emitting laser devices. Wet chemical etching mesa structure is generally used.

Figure 30 shows the laser power current characteristics at different temperatures. The test setup is similar as mentioned earlier. The collected peat power at 80 K is about 80 mW/Facet. And the highest lasing temperature is 180 K. The external quantum efficiency is ~90% at 80K and dropped to ~40% at 180K. The characteristic temperature T_0 for most of the devices tested is about 40 K. Although the device performance is still away from the satisfaction, we do made good progress based on all of improvements on material development and device processing.

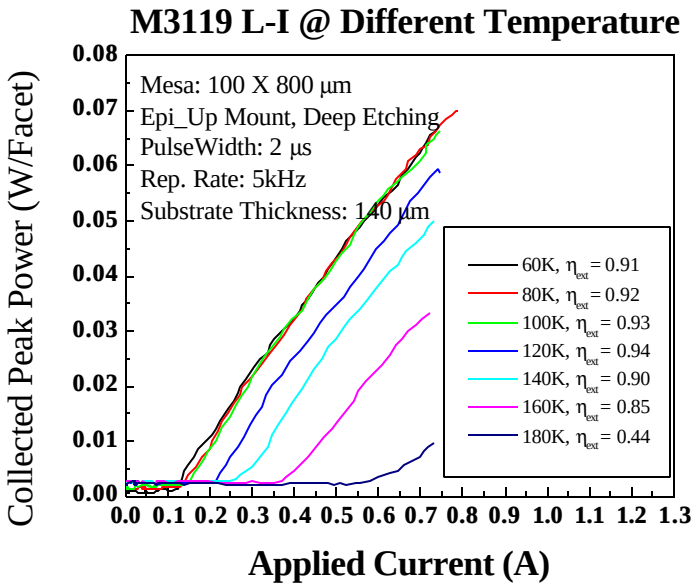

L-I characterization of the Electrically Pumped (EP) type-I lasers

In the progress of developing multi-color quantum cascade mid-IR sources in 2.5 to 5 μm, we have evaluated the different possible structures and technologies. Beside the development reported in previous sections with type-II QC lasers, we are also investigating the possibility of using type-I QC laser structure to develop the mid-IR emission in the wavelength regions (4 to 5 μm). L-I curves shown in Figure 31 demonstrated that the laser device has excellence performance under pulsed mode operation. The highest temperature at the pulse mode has reached 340K which is above room temperature.

The threshold current density has been plotted at various temperatures in Figure 32. Assuming that the actual active region is 12 μm wide, with a 2 mm long device, we found that the characteristic temperature of T_0 is about 114K.

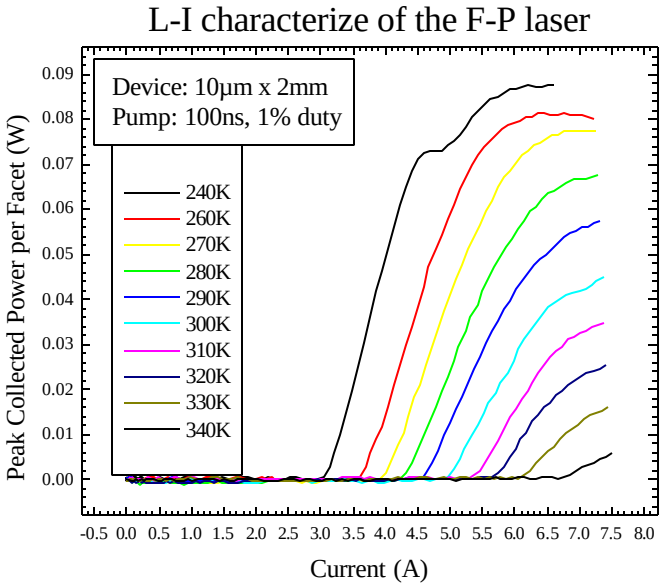

Figure 31. L-I characteristics of the 5.2 mm Type-I QC lasers.

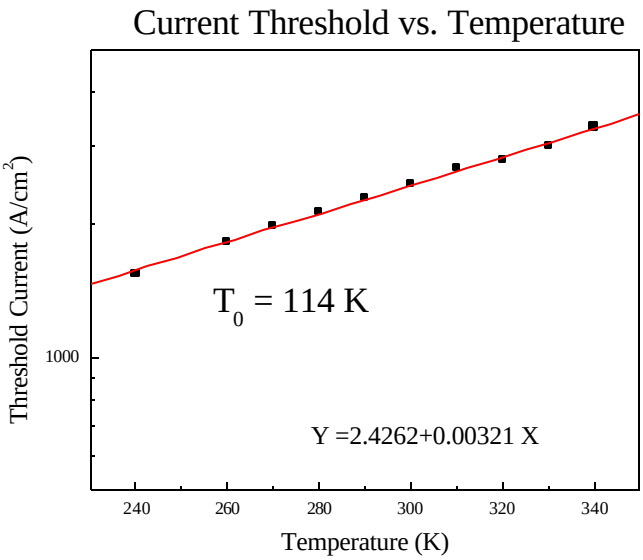

Figure 32. Threshold current density vs. temperature.

Spectral characterizations

Spectral characterizations of the Electrically Pumped (EP) type-II lasers

The test setup for laser device mounting and cryostat temperature facility are similar as mentioned earlier. Laser spectrum has been measured with a CVI ¼ meter monochromator coupled with an liquid nitrogen cooled InSb photodiode detector. The lasing spectra at different submount temperatures are demonstrated in Figure 33. The measured laser wavelengths are within good agreement with the design and demonstrated a wide tunable range with the development of DBR grating.

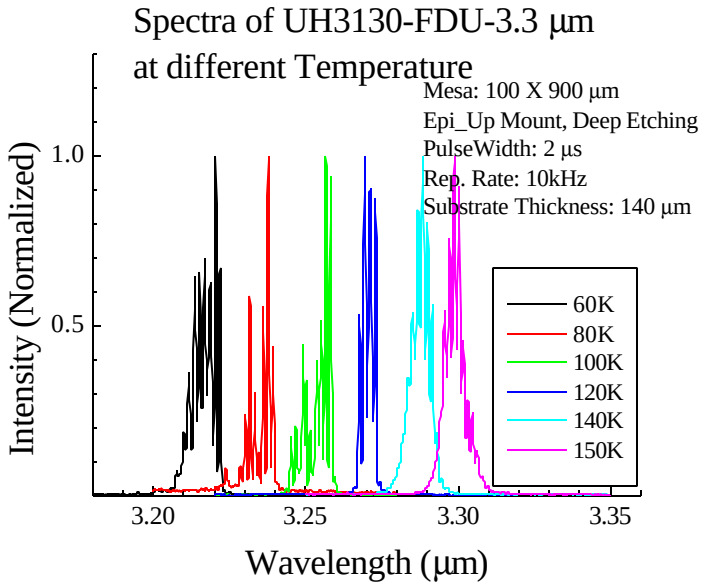

Spectral characterizations of the Electrically Pumped (EP) type-I lasers

The spectrum of the electrically pumped type-I QC lasers at various temperatures have been measured with an ½ m monochromator coupled with an liquid nitrogen cooled InSb photodiode detector. The lasing spectra at different submount temperatures of the FP lasers are demonstrated in Figure 34.

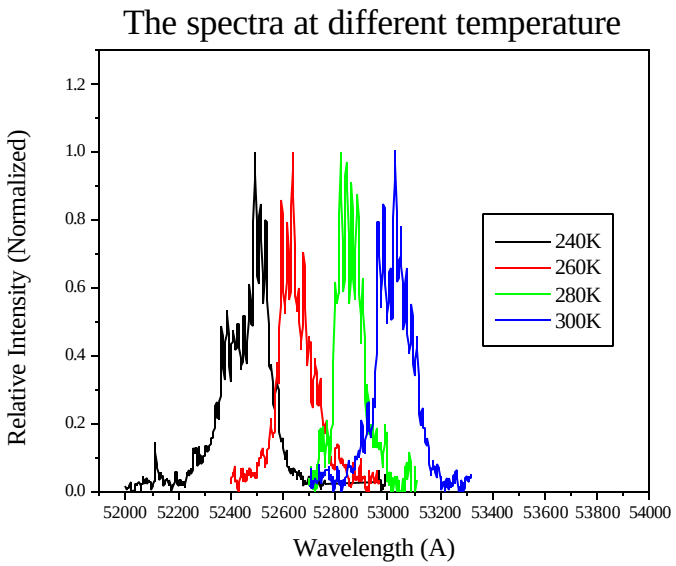

Figure 34. Lasing spectra at different temperatures.

A high resolution spectrum collected with the CVI ½ m monochromator is shown in Figure 35. The F-P modes are clearly demonstrated.

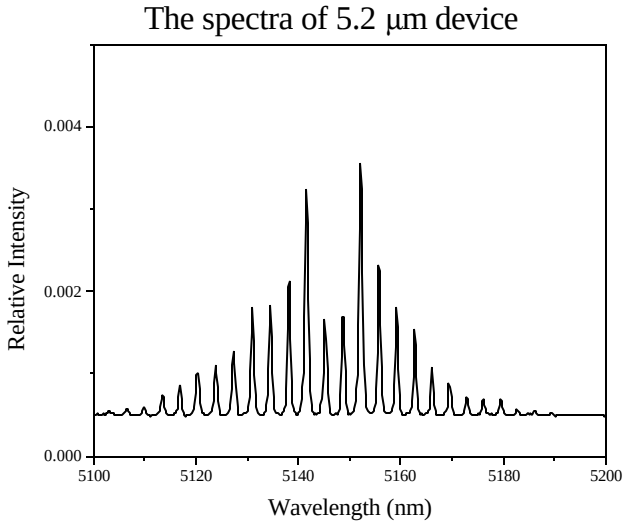

Figure 35. High resolution lasing spectrum at 120 K.

The spectra of the 5.2 μm laser device were collected with a 1/4 m CVI monochromator coupled with a liquid nitrogen cooled InSb photodiode detector. Spectra were obtained at different applied currents at 140 K, CW mode, at

different temperatures at both CW and Pulse mode. Figure 36 shows the spectra at different applied currents at a submount temperature of 140 K. The spectra were taken just above the threshold current with a slits width of 50 μm.

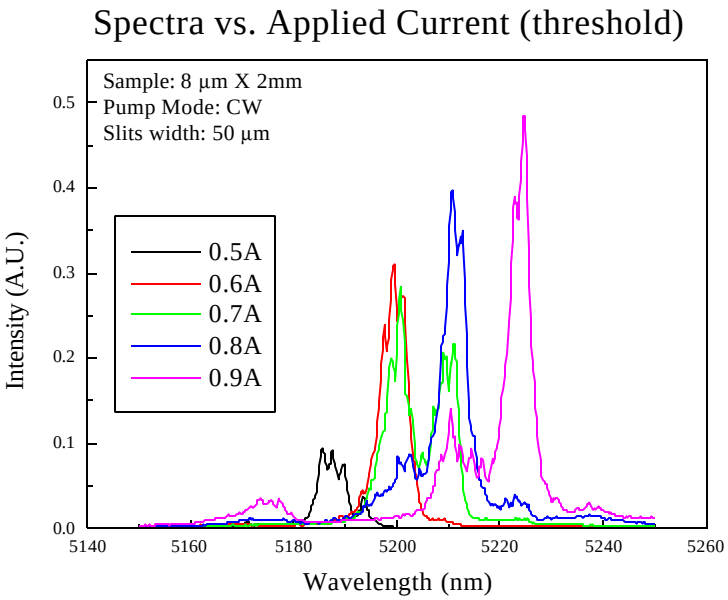

Figure 37 demonstrates the spectra at different submount temperatures under pulsed mode operation. The spectra were collected just above the threshold current. AOI laser driver was used to supply the 25 ns short pulses with a repetition rate of 1 kHz. The spectra at 180K, 200K and 220K have almost the same maximum. The reason is not exactly known. Therefore, more testing has planned to gain a better understanding.

The lasing spectra maximum vs. temperature has also been plotted in Figure 38 for both CW and pulsed mode operations. From the figure, we can see that the lasing wavelengths covering a wide range. This could provide us a good temperature tuning characteristics.

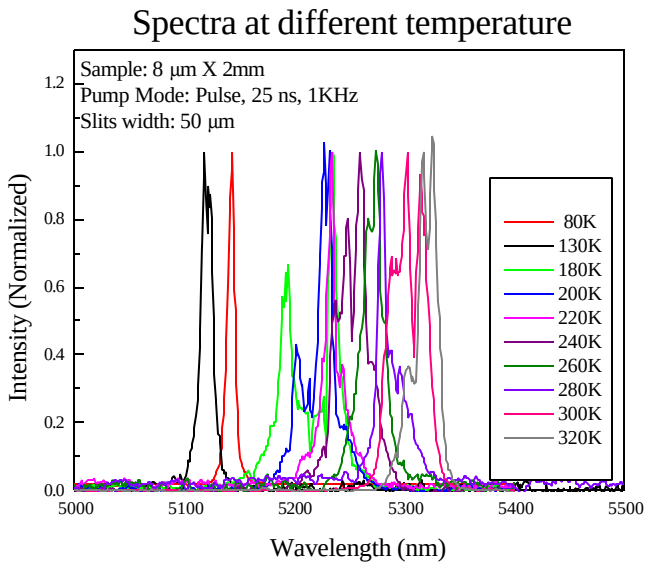
Spectra at different temperature
Sample: 8 μm X 2mm
Pump Mode: Pulse, 25 ns, 1KHz
Slits width: 50 μm
Intensity (Normalized)
Wavelength (nm)
80K
130K
180K
200K
220K
240K
260K
280K
300K
320K

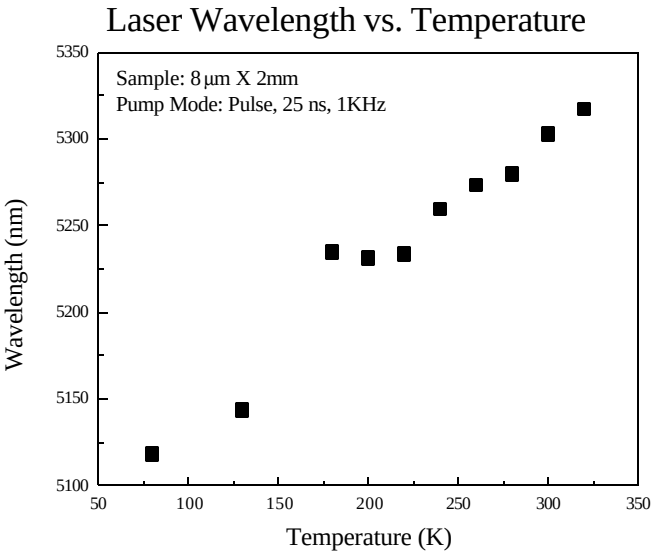
Laser Wavelength vs. Temperature
Sample: 8 μm X 2mm
Pump Mode: Pulse, 25 ns, 1KHz
Wavelength (nm)
Temperature (K)

5.0 Synergistic interaction with other programs

As stated in the program plan, synergistic interaction of this program with other concurrent programs on other advanced technology and system development is a major aspect of this effort. Two specific programs with direct bearing on this programs are tunable mid-IR lasers and advanced lidar systems. This section reviews these synergistic efforts and their impact on this program.

Tunable mid-IR lasers.

The broadly tunable mid-IR laser effort is aiming for spectroscopic sensing applications (i.e., Fig. 39). A specific task is to evaluate and optimize the gain band, threshold, and efficiency of mid-IR materials. A phase of the evaluation is to develop a laboratory-based grating-tuned external cavity. This phase has been achieved in the past quarter. The result is summarized in the following [32].

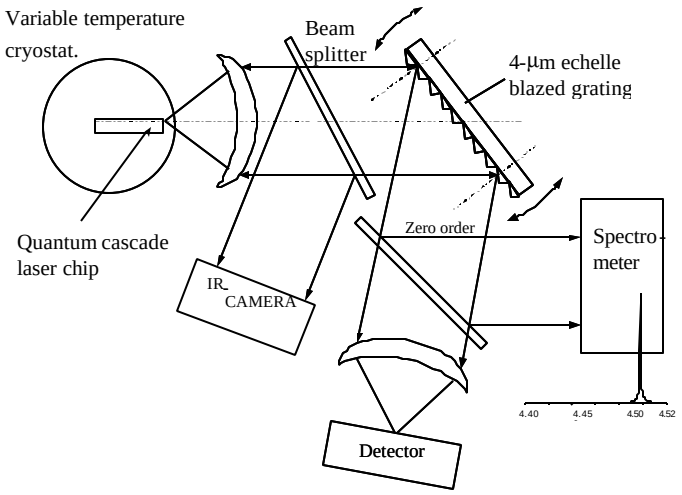

Fig. 39. Configuration of external cavity tunable lasers.

The wavelength tuning property of mid-IR laser can be evaluated using grating-coupled external cavity. Such a cavity has been developed and for the testing purpose, InGaAs/InAlAs type-I quantum cascade lasers were used (as shown in Figure 40). An objective is to determine the optimal condition for threshold and power efficiency as a function of wavelength and temperature. Knowledge of these conditions can help choosing a wafer design for which a DFB or DBR laser can be fabricated for a

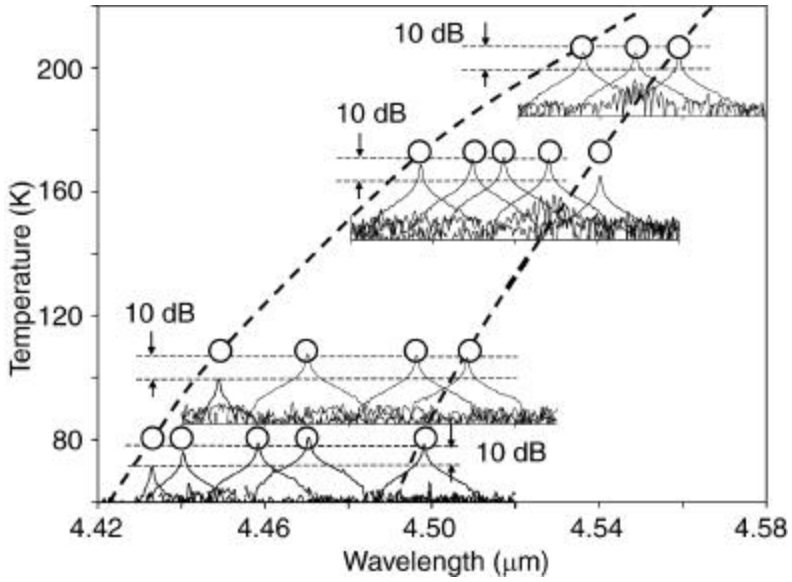

Fig. 40. Wavelength tuning range vs. temperature (dashed curve). Each open circle indicates the temperature and wavelength for which L-I and I-V were measured. The corresponding lasing spectrum is shown underneath, and the 10 dB scale is also shown.

specific wavelength and temperature range. The materials were grown by MBE and fabricated into 4-7-μm-wide, 0.5-2-mm-long ridge-waveguide lasers. Typical free-running power was ~ 350 mW peak at 80 K and ~ few 10's mW above 220K.

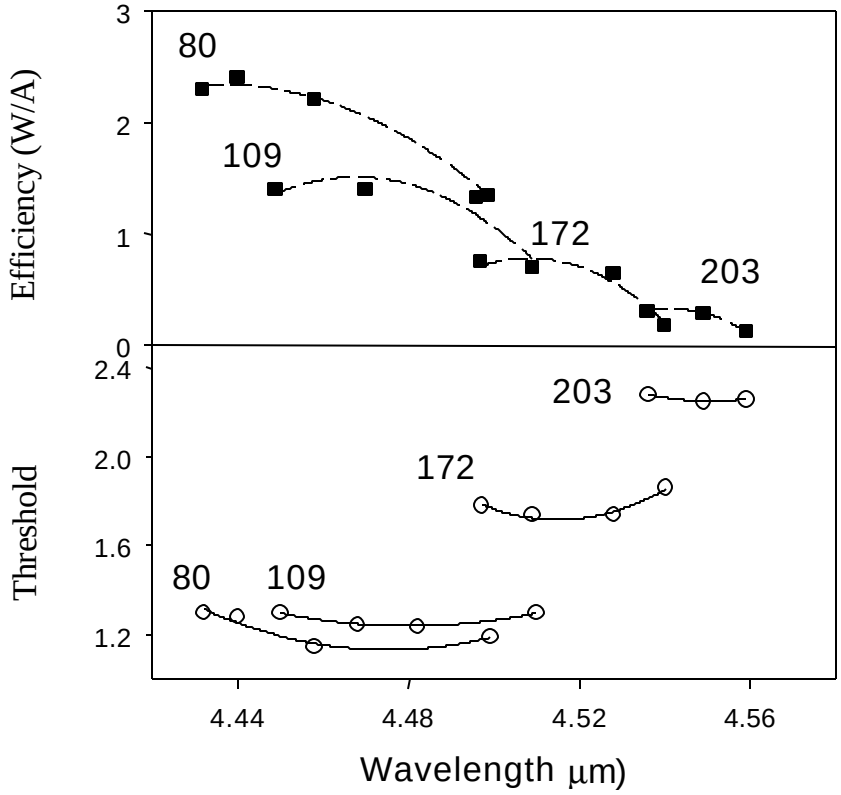

Figure 41 Wavelength dependence of threshold (circles with
efficiency (squares with dashed lines) at different operating temperatures

Uncoated lasers with free-running wavelength of 4.5 and 5.1 μm were inserted in an external cavity configuration shown in Fig. 39. The lasers were operated with 100 to 500-ns pulses and 100-500-kHz repetition rate. The temperature was varied from 80 to 230 K. The grating was used in the first order for feedback and zeroth order for output. All devices exhibited single axial mode; some narrow ridges had TEM_{00} and allowed efficient external grating feedback, while wider ridges had TEM20 mode with less efficient coupling and tuning range. The tuning range was defined as the limits of grating-selectable wavelength for which the free-running laser power was suppressed to < 20 dB of the grating-selected power. The curves shown in Fig. 41 shows a 65-nm tuning range at 80 K, which tapered to 23 nm at 203 K; reflecting the narrowing of QC laser gain band with increasing temperature. Within each range, every wavelength where a monolithic device Fabry-Perot mode and the grating-cavity longitudinal mode coincide was accessible. The open circles correspond the wavelengths for which L-I and I-V curves were measured. Beneath each circle is the

corresponding spectrum. The linewidth of single mode was narrower than the 4-GHz spectrometer resolution; however, 2 or 3 longitudinal modes were sometimes observed at high power.

A key observation is that for every temperature range, the wavelength for highest lasing efficiency is consistently shorter than that of free-running devices, as shown in Fig. 41. The threshold varied slightly vs. wavelength (Fig. 41(b)), but the efficiency was more optimal for short wavelength (Fig. 41(a)). The I-V curves also showed an observable lower voltage for shorter wavelength at the same drive current. Qualitatively, the lower voltage-shorter wavelength effect can indicate that as the laser is forced to operate at higher photon energy, the electrons have less energy to relax between stages and thus, resulting in a lower voltage drop across each injection stage. Stimulating hot electrons to radiate can also conceivably compete with phonon-emitting relaxation for higher carrier-recycle efficiency. Additionally, the results in Figs. 39 and 40 suggest that for a DFB or DBR laser of a specific desirable wavelength to operate efficiently over a wide temperature range, the gain band can be designed toward longer wavelength.

Advanced code-division multiplexing lidar.

System development is not a part of this program. However, the goal of this program is to develop enabling technology for applications, and one particular application is spectral lidar for remote sensing. A synergistic program at University of Houston is to develop a concept for short-range spectral lidar using low power mid-IR lasers. The effort provides a framework to evaluate and extrapolate to higher power lidars using the technology in this effort.

A short-range spectral lidar based on the code-division multiplexing (CDM) architecture using mid-infrared Sb semiconductor lasers for remote sensing has been demonstrated with near detector-limited performance. The system principle is similar to optical-CDMA

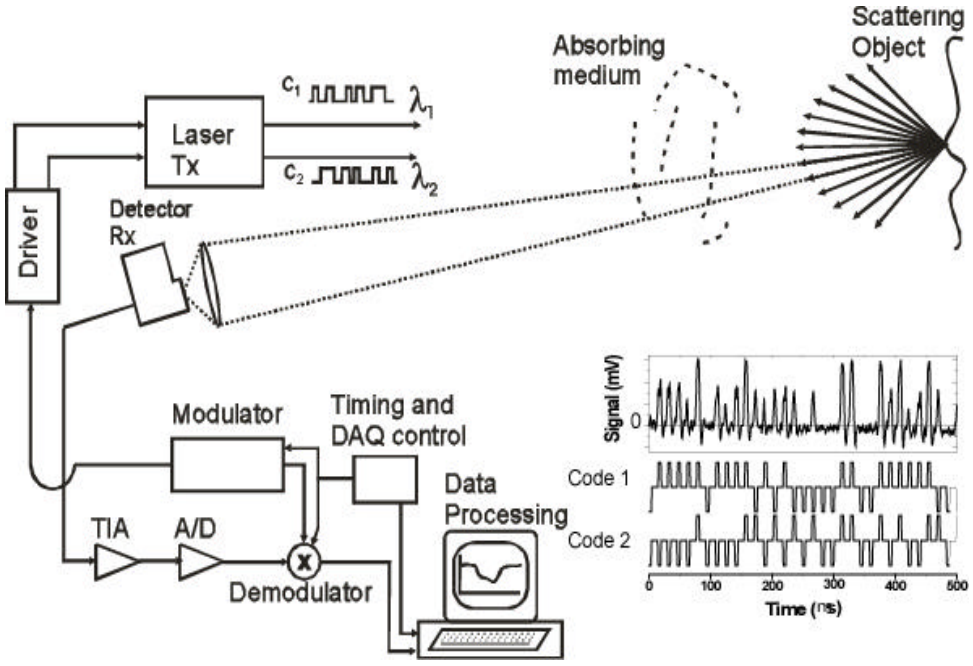

Fig. 42. System block diagram.

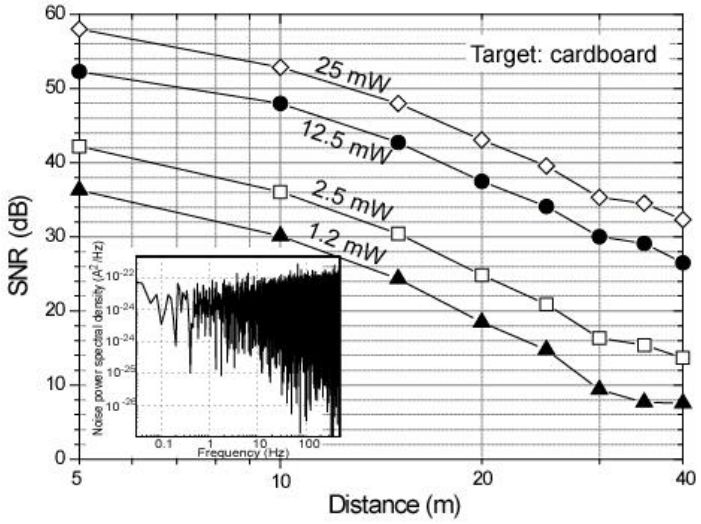

Figure. 43. Return signal-to-noise ratio (1 kHz-bandwidth) vs. distance for different transmitter power. The inset shows the power spectral density of the demodulated system noise (absence of optical signal), which has a white-Gaussian-like spectrum with very little l/*f*.

for communications and applicable to any number of wavelengths, but was demonstrated with two wavelengths similarly to conventional DIAL. An experiment using < 20-mW transmitter average power could detect an open-air acetylene gas leak from 10 m away with dynamic, random, non-cooperative backscatters. It can distinguish hydrocarbon oil from organic oil slick on water. We believe this is among the first demonstrations of this semiconductor spectral lidar with orthogonal CDM architecture, as well as the first demonstration of mid-IR Sb lasers used in open path, non-cooperative target remote sensing.

Figure 42 illustrates the experiment. The transmitter consists of a 3.1 and 3.7-μm Sb laser; each was intensity-modulated with a unique, 2-level {1,0}, 2^N-chip-length pseudo-noise codes that are elements of a basis set $\left\{\left\{C_{i,k}\right\}_{i=1}^{2^N}\right\}_{k=1}^{2^N-1}$. A key feature of this CDM that is suitable for lidar, and different from O-CDMA, is that the receiver does not use the same $C_{i,,k}$'s to demodulate the back-scattered power, which cannot have perfect orthogonality and lead to non-vanishing intercode correlation. Instead, the decoding uses 3-level {-1,0,1} functions $D_{j,,m} \in \left\{\left\{D_{j,m}\right\}_{j=1}^{2^N}\right\}_{m=1}^{2^N-1}$ that are truly orthogonal to $C_{i,,k}$, such that:

$$\sum_{i=1}^{2^N} C_{i,k} D_{i,m} = P\, d_{k,m}\,,\ \forall k,m\,;$$

$$\left|\sum_{i=1}^{2^N} C_{i,k} D_{i+q,m}\right| << P\,,\ \forall\, q \neq 0, k, m\,;$$

and

$$\sum_{i=1}^{2^N} D_{i,m} = 0,\ \forall m$$

where *P* is a constant integer. This approach reduces channel crosstalk to shot-noise-

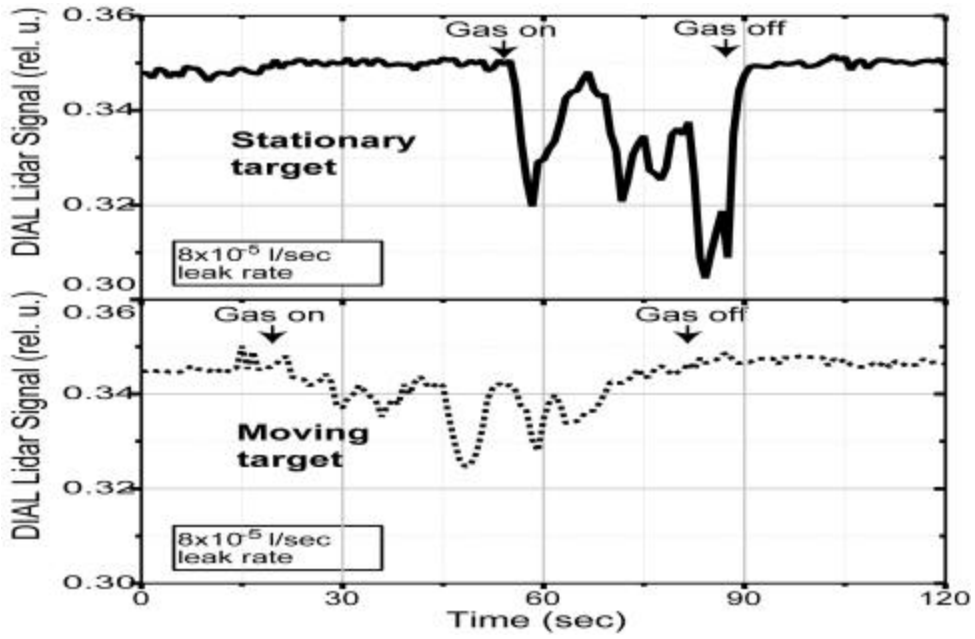

Fig. 44. Acetylene absorption signature obtained as the ratio of the 3.1- vs. 3.7-μm return signal from 10 m away for: (top) with a stationary background object; and (bottom) an moving target. The estimated return signal.

limited level, and filters out both impulse noises and low-frequency noises such as 1/*f*. Both RZ and NRZ signaling formats can be used. An example of a RZ signal with the two corresponding decoding functions are shown in Fig. 42 inset.

Figure 43 shows the return SNR (square-law detector signal power) as a function of backscatterer distance and transmitter power for 1-ms integration time. The cardboard target has a backscattering coefficient ~average among various man-made surfaces studied. The results showed that a mere 25-mW average transmitter power and a 7.5-cm-diameter aperture receiver gave a 30-dB SNR return signal from a target 40 m away. With 1-kHz sampling rate, the system could easily see dynamic targets up to 500-Hz bandwidth. The noise is limited by the fundamental detector noise. More importantly, the inset shows a white-Gaussian-like power spectral density for the decoded receiver noise with very little discernible 1/*f* component.

The system was demonstrated with acetylene, which absorbs 3.1 but not 3.7-μm radiation. The transmitter 20-mW total power, 15-cm-wide beams were introduced within a 20-cm vicinity of a $<8x10^{-5}$-liter/sec (at STP) leak (0.01 ft^3/hour) at 10 m away with a moving non-cooperative backscatterer (concrete surface) in the background. The ratio of the return signals in Fig. 44 shows a clear signature of the leak. The solid curve was for a moving and the dashed curve was for a stationary backscatterer. For both, the leak SNR is 14 dB with 0.1-sec integration time per sampling point. The difference between the moving and stationary object signal amplitudes was probably due to a larger dispersion the leaked gas by the moving object.

This experiment demonstrates the future feasibility of handheld, short-range spectral lidars using compact, mW-range semiconductor mid-IR lasers. For this program which aims to develop higher power laser, 100's-mW to Watt-class lasers, a focus is to achieve high bandwidth and low noise for km-range detection. This synergistic effort can provide testing necessary for optimization. Mid-IR Sb lasers developed under this DUST program are anticipated to be evaluated in the forth and fifth quarters.

6.0 Discussions

This project is a vertically integrated developmental effort to realize a user-ready mid-IR semiconductor laser subsystems. It is designed to exploit the latest advances in Sb lasers and type-I QC lasers, explore its potential and limitation within the larger framework of system deployment. It is conceived by a team of organizations with complementary technical expertise and vested interest in bringing this technology to the market place. Interest in advanced science and technology and business opportunity are merged into a common perspective to formulate the project goal, guideline, and framework.

We have achieved very good results in terms of high temperature continuous wave (CW) operation of type I quantum cascade lasers at 5.2 μm. The new laser device has demonstrated more than 8 milliwatts of cw power at a temperature of -63 ºC (-81 F). This temperature is achievable with the use of small, relatively inexpensive, thermoelectric coolers, rather than bulky and expensive cryogenically cooled systems. The improved temperature performance is due to improved device characteristics as illustrated by the high T_0, the low J_0 and a low operating voltage. The measured thermal resistance is quite large compared to theoretical calculations and what others have reported, however if the thermal resistance can be lowered, the maximum CW operating temperature could reach as high as 280K.

We have made much progress in material development, laser device processing and packaging, especially on the understanding of the material and device processing towards manufacturing. A great effort has been devoted to the process manufacture facility (i.e., clean room construction, process equipment installation and testing, etc.). Many progress have been made in quality control (QC) to improve the yield. Material characterization methodologies, such as wafer level testing both in-situ and non-destructive, have been developed.

References:

1. H. K. Choi and S. J. Englash, Appl. Phys. Lett. 59, 1165 (1992).
2. H. Q. Le, G. W. Turner, S. J. Eglash, H. K. Choi, and D. A. Coppeta "High-power diode-laser-pumped InAsSb/GaSb and GaInAsSb/GaSb lasers emitting from 3 to 4 μm" Appl. Phys. Lett. **64**, 152 (1994).
3. S. R. Kurtz, R. M. Biefeld, L. R. Dawson, K. C. Baucom, and A. J. Howard, "Midwave (4.5 μm) infrared lasers and light-emitting diodes with biaxially compressed InAsSb active regions," Appl. Phys. Lett., Vol. **64**, pp. 812-814, (1994).
4. H. Q. Le, G. W. Turner, J. R. Ochoa, H. K. Choi, J. M. Arias, M. Zandian, R. R. Zucca, and Y.-Z. Liu "High-power diode-pumped mid-infrared semiconductor lasers," Proc. SPIE **2382**, 262 (1995).
5. H. K. Choi, G. W. Turner, and M. J. Manfra "High CW power (> 200 mW/facet) at 3.4 μm from InAsSb/InAlAsSb strained quantum well diode lasers," Electron. Lett. **32**, 1296 (1996).
6. H. Q. Le, G. W. Turner, V. Daneu, J. R. Ochoa, H. K. Choi, A. Sanchez, D. L. Spears, and T. Y. Fan, Proceedings of 1996 IRIS Symposium, Baltimore, ERIM, Michigan, (1996)
7. A. Popov, V. Sherstnev, Y. Yakovlev, R. Mucke, and P. Werle, "High power InAsSb/InAsSbP double heterostructure laser for continuous wave operation at 3.6 μm," Appl. Phys. Lett. **68**, 2790 (1996).
8. J. I. Malin, J. R. Meyer, C-H. Lin, P.-C. Chang, S. J. Murry, R. Q. Yang, and S.-S. Pei, "Type-II mid-infrared quantum well lasers," Appl. Phys. Lett. **68**, 2976 (1996).
9. J. I. Malin, C-H. Lin, P.-C. Chang, S. J. Murry, and S.-S. Pei, "Type-II mid-IR lasers operating above room temperature," Electron. Lett. **32**, 1593 (1996).
10. H. Q. Le, G. W. Turner, J. R. Ochoa, M. J. Manfra, C. C. Cook, and Y.-H. Zhang "Broad wavelength tunability of grating-coupled external cavity mid-infrared semiconductor lasers" Appl. Phys. Lett. **69**, 2804 (1996).
11. T. C. Hasenberg, D. H. Chow, A. R. Kost, R. H. Miles, and L. West, "Demonstration of 3.5 μm Ga1-xInxSb/InAs superlattice diode laser," Electron. Lett. 31, 275 (1995); R. H. Miles, T. C. Hasenberg, A. R. Kost, and L. West, "GaInSb/InAs superlattice-based infrared lasers," Proc. SPIE 2694, 2 (1996).
12. C.-H. Lin, P. C. Chang, S. J. Murry, D. Zhang, Yucai Zhou, and S. S. Pei at SVEC, J. I. Malin et al. at NRL, "Nearly Room-Temperature Type-II Quantum-Well Lasers at 3-4 μm", J. Electronic Materials, vol. 26, pp. 440-443, (1997).
13. C.-H. Lin, R. Q. Yang, D. Zhang, S. J. Murry, and S. S. Pei, A. A. Allerman, and S. R. Kurtz, "Type-II Interband Quantum Cascade Lasers at 3.8 μm", Electron. Lett., vol. **33**, pp. 598-599, (1997).
14. B. Lane, D. Wu, H. Yi, J. Diaz, A. Rybaltowski, S. Kim, M. Erdtmann, H. Jeon, and M. Razeghi, Appl. Phys. Lett. **70**, 11 (1997).
15. C.-H. Lin, P. C. Chang, S. J. Murry, D. Zhang, Yucai Zhou, and S. S. Pei at SVEC, J. I. Malin et al. at NRL, "Nearly Room-Temperature Type-II Quantum-Well Lasers at 3-4 μm", J. Electronic Materials, vol. **26**, pp. 440-443, 1997.
16. C.-H. Lin, P. C. Chang, S. J. Murry, D. Zhang, Yucai Zhou, and S. S. Pei at SVEC , J. I. Malin, and J. R. Meyer at NRL, "MBE Grown Mid-Infrared Type-II Quantum-Well Lasers", J. Crystal Growth, vol. **175**, pp. 955-959, 1997.
17. C.-H. Lin, R. Q. Yang, S. J. Murry, and S. S. Pei, C. Yan, D. L. McDaniel, and M. Falcon, "Room-Temperature Low-Threshold Type-II Quantum-Well Lasers at 4.5 μm", IEEE Photon. Technol. Lett., vol. **9**, pp. 1573-1575, (1997).

18. A. N. Baranov, N. Bertru, Y. Cuminal, G. Boissier, C. Alibert, and A. Joullie, "Observation of room-temperature laser emission from type III InAs/GaSb multiple quantum well structures," Appl. Phys. Lett. **71**, 735 (1997).
19. R. Q. Yang, B. H. Yang, D. Zhang, C. H. Lin, S. J. Murry, H. Wu, and S. S. Pei, "High Power Mid-IR Interband Cascade Lasers Based on Type-II Quantum Wells", Appl. Phys. Lett., vol. **71**, pp. 2409-2411, 1997.
20. D. Z. Garbuzov, R. U. Martinelli, H. Lee, R. J. Menna, P. K. York, L. A. Dimarco, M. G. Harvey, R. J. Materese, S. Y. Narayan, and J. C. Connolly, "4 W quasi-continuous-wave output power from 2-μm AlGaAsSb/InGaAsSb single-quantum-well broadened waveguide laser diodes," Appl. Phys. Lett. **70**, 22 (1997).
21. B. H. Yang, D. Zhang, R. Q. Yang, C. H. Lin, S. J. Murry, and S. S. Pei, "Mid-IR Interband Cascade lasers with Quantum Efficiencies > 200%", Appl. Phys. Lett., vol. **72**, pp. 2220-2222, (1998).
22. H. Q. Le, G. W. Turner, J. R. Ochoa, and H. K. Choi, C. H. Lin, R. Q. Yang, and S. S. Pei, "Efficiency and power issues in Sb-based mid-infrared lasers", Proceeding of SPIE, Vol. **3284**, p. 276 (1998).
23. H. Q. Le, C. H. Lin, S. J. Murray, R. Q. Yang, and S. S. Pei, "Effects of the internal loss on power efficiency of InAs/GaInSb/AlSb QW lasers and comparison with InAsSb lasers", IEEE J. of Quant. Electron. **QE-34**, 1016 (1998).
24. C. H. Kuo, C.-H. Lin, C. H. Thang, S. S. Pei, and Y. C. Zhou, "High-Power Mid-IR Type-II Quantum Wells Lasers Grown on Compliant Substrates", Apply. Phys. Lett. (to appear).
25. Faist, J., F. Capasso, D. L. Sivco, C. Sirtori, A. L. Hutchinson, and A. Y. Cho, *Science* **264**, 553 (1994).
26. Faist, F. Capasso, C. Sirtori, A. L. Hutchinson, D. L. Sivco, J. N. Baillargeon, A. L. Hutchinson, S.-N. G. Chu, and A. Y. Cho, "High power mid-infrared (l ~ 5 μm) quantum cascade lasers operating above room-temperature," Appl. Phys. Lett. **68**, 3680 (1996).
27. J. Faist et al., presented at CLEO/QELS '97, Baltimore, MD, (1997).
28. Faist, J., C. Gmachl, F. Capasso, C. Sirtori, D. L. Sivco, J. N. Baillargeon, A. L. Hutchinson, and A. Y. Cho, *Appl. Phys. Lett*. **70**, 2670 (1997).
29. Namjou, K., S. Cai, E. A. Whittaker, J. Faist, C. Gmachl, F. Capasso, D. L. Sivco, and A. Y. Cho, *Opt. Lett*. **23**, 219-221 (1998).
30. Faist, J., F. Capasso, D. L. Sivco, C. Sirtori, A. L. Hutchinson, M. Beck, S. N. G. Chu, and A. Y. Cho, *Appl. Phys. Lett*. **72**, 680 (1998).
31. Brain Ishaug, Wen-Yen Hwang, Jae Um, Bujin Guo, Hao Lee, and Chih-Hsiang Lin, "Continuous-wave operation of a 5.2 mm quantum-cascade laser up to 210 K", Applied physics Letters, **79**, 1745-1747, 2001.
32. G.P. Luo, C. Peng, H.Q. Le, and S.S. Pei, W.-Y. Hwang, B. Ishaug, J. Um, James N. Baillargeon, and C.-H. Lin, "Grating-tuned external-cavity quantum-cascade semiconductor lasers", Applied Physics Letters, **78**, 2834-2846, 2001.

Appendix A

Summary of the wafer growth

Wafer #	Design (80K)	Type of structure	Peak Power (/Facet)	Comments
2959	3.3 µm	Type-II QW		OPLD
2968	3.3 µm	Type-II QW		OPLD, No PL
2975	3.3 µm	Type-II QW		OPLD, No PL
2985	3.3 µm	Type-II QW		OPLD, No PL
2999	3.3 µm	Type-II SL		
3000	3.3 µm	Type-II SL		
3001	3.18 µm	Type-II QW		OPLD, PL=3.8 µm
3002	3.9 µm	Type-II QW		OPLD, PL=3.85 µm
3003	3.3 µm	Type-II SL		
3006	3.3 µm	Type-II SL		
3007	3.08 µm (150 K)	Type-II QW		OPLD, PL=3.3 µm (300K)
3012	3.3 µm	Type-II SL		
3013	3.23 µm (150 K)	Type-II QW		OPLD, PL=3.23 µm (150K)
3014		Type-II SL		Calibration
3020	3.3 µm	Type-II SL		
3026	3.3 µm (120 K)	Type-II QW		OPLD, PL=3.42 µm (150K)
3039	3.3 µm	Type-II SL		Growth rate low
3040	3.3 µm (300K)	Type-II SL		PL = 3.4 µm (77K)
3047		Type-II OP		Test on compliant substrate
3050	3.3 µm	Type-II QW		
3054	3.3 µm	Type-II SL		defect, Chamber Open
3056	3.9 µm	Type-II OP		Calibration
3106	4.0 µm			Weak output power
3112	3.79 µm		40 mW	
3114	4.18 µm		65 mW	
3119	3.8 µm	QC	80 mW	Best performance
3128	3.2 µm	QC	40 mW	Low threshold
3130	3.2 µm	SL	15 mW	High internal loss

Appendix A (continued)

Wafer #	Design (80K)	Type of structure	Peak Power (/Facet)	Comments
3166	3.6 μm			Weak output power
3169	3.7 μm			Weak output power
3171	3.6 μm	OP		
3173	3.3 μm	SL		
3176	3.3 μm	SL		
3178	3.3 μm	SL		
3197	3.3 μm	SL		
3200	3.3 μm	SL		
3202	3.3 μm	SL		
3203	3.3 μm	SL		
A0132	4.6 μm	Type-I QC		
A0133	4.6 μm	Type-I QC		
A0138	4.6 μm	Type-I QC		Shutter problem
A0140	5.225 μm	Type-I QC		
A0147	4.6 μm	Type-I QC		
A0148	4.6 μm	Type-I QC		
A0149	4.6 μm	Type-I QC		
A0151		InGaAs/InAlAs		Calibration
A0153	4.6 μm	Doping calibration(Si)		Calibration
A0156	4.6 μm	Type-I QC		
A0158	4.6 μm	Type-I QC		
A0159	4.6 μm	Type-I QC		Aborted, computer problem
A0160	4.6 μm	Type-I QC		
A0162	4.6 μm	Type-I QC		
A0163	4.6 μm	Type-I QC		
A0164		Si Doping		Calibration
A0170	5.2 μm	Type-I QC		
A0171	5.2 μm	Type-I QC		
A0173	5.2 μm	Type-I QC		
A0175	5.2 μm	Type-I QC		
A0177	4.6 μm	Type-I QC		
A0176	4.6 μm	Type-I QC		
A0177	4.6 μm	Type-I QC		
A0189	4.6 μm	Type-I QC		
A0190	4.6 μm	Type-I QC		
A0204	5.2 μm	Type-I QC		
A0217	4.6 μm	Type-I QC		
A0259	4.6 μm	Type-I QC		

Appendix A (continued)

Wafer #	Design (80K)	Type of structure	Peak Power (/Facet)	Comments
A0270	5.2 μm	Type-I QC		
A0272	5.2 μm	Type-I QC		

DISTRIBUTION LIST

DTIC/OCP 8725 John J. Kingman Rd, Suite 0944 Ft Belvoir, VA 22060-6218	1 cy
AFRL/VSIL Kirtland AFB, NM 87117-5776	1 cy
AFRL/VSIH Kirtland AFB, NM 87117-5776	1 cy
Applied Optoelectronics, Inc. 13111 Jess Pirtle Blvd. Sugar Land, TX 77478	1 cy
Official Record Copy AFRL/DELS/2d Lt Rob Hill	3 cys